BRAF^{V600E} induces reversible mitotic arrest in human melanocytes via microRNA-mediated suppression of AURKB.

Andrew S. McNeal[1], Rachel L. Belote[2,], Hanlin Zeng[2,], Marcus Urquijo[2], Kendra Barker[2], Rodrigo Torres[1,3], Meghan Curtin[2], A. Hunter Shain[1,3], Robert H. I. Andtbacka[2,4], Sheri L. Holmen[2,4,5], David H. Lum[2], Timothy H. McCalmont[6], Matthew W. VanBrocklin[2,4,5], Douglas Grossman[2,5,7], Maria L. Wei[1,3,8], Ursula E. Lang[1,3,6], and Robert L. Judson-Torres[2,5,7,†]

[1] Helen Diller Family Comprehensive Cancer Center, University of California San Francisco, San Francisco, CA, 94158, USA.
[2] Huntsman Cancer Institute, University of Utah, Salt Lake City, UT, 84112, USA.
[3] Department of Dermatology, University of California San Francisco, San Francisco, CA, 94115, USA.
[4] Department of Surgery, University of Utah, Salt Lake City, UT, 84132, USA.
[5] Department of Oncological Sciences, University of Utah, Salt Lake City, UT, 84132, USA.
[6] Department of Pathology, University of California San Francisco, San Francisco, CA, 94143, USA.
[7] Department of Dermatology, University of Utah, Salt Lake City, UT, 84102, USA.
[8] San Francisco Veterans Affairs Medical Center, San Francisco, San Francisco, CA, 94121, USA.

† To whom correspondence should be addressed. Tel: +1 801-213-8436; Email: judsontorreslab@gmail.com

Abstract

Benign melanocytic nevi frequently emerge when an acquired *BRAF^{V600E}* mutation triggers unchecked proliferation and subsequent arrest in melanocytes. Recent observations have challenged the role of oncogene-induced senescence in melanocytic nevus formation, necessitating investigations into alternative mechanisms for the establishment and maintenance of proliferation arrest in nevi. We compared the transcriptomes of melanocytes from healthy human skin, nevi, and melanomas arisen from nevi and identified a set of microRNAs as highly expressed nevus-enriched transcripts. Two of these microRNAs – MIR211-5p and MIR328-3p – induced mitotic failure, genome duplication and proliferation arrest in human melanocytes through convergent targeting of AURKB. We demonstrate that *BRAF^{V600E}* induces a similar proliferation arrest in primary human melanocytes that is both reversible and conditional. Specifically, *BRAF^{V600E}* expression stimulates either arrest or proliferation depending on the differentiation state of the melanocyte. We report genome duplication in human melanocytic nevi, reciprocal expression of AURKB and microRNAs in nevi and melanomas, and rescue of arrested human nevus cells with AURKB expression. Together, our data describe an alternative molecular mechanism for melanocytic nevus formation that is congruent with both experimental and clinical observations.

Introduction

Cutaneous melanoma is a potentially deadly skin cancer arising from the pigment-producing melanocytes of the human epidermis. An activating mutation in the BRAF proto-oncogene ($BRAF^{V600E}$) drives over half of all cutaneous melanomas[1–3]. Yet, when a melanocyte acquires a $BRAF^{V600E}$ mutation, the cell does not immediately transform to cancer. Instead, it usually undergoes clonal proliferation followed by stable arrest resulting in a benign skin lesion known as a melanocytic nevus or "mole"[3–6]. Despite the continued expression of $BRAF^{V600E}$, the majority of melanocytic nevi remain innocuous for the lifespan of the individual, suggesting that nevus cells have robust intrinsic defenses against hyperproliferation. By inducing hyperproliferation and subsequent arrest, the $BRAF^{V600E}$ mutation elicits divergent, biphasic phenotypes within a single cell – a poorly understood phenomenon. Characterization of the mechanisms and environmental factors that distinguish the two phenotypes could illuminate candidate strategies for chemoprevention of melanocytic nevus formation or interception of melanoma initiation.

The $BRAF^{V600E}$ mutation is clonally present in ~80% of human melanocytic nevi[3] and melanocyte-specific expression of the oncogene is sufficient to induce nevus formation in mice[6–8], suggesting that $BRAF^{V600E}$ drives proliferation arrest in melanocytes. The prevailing theory to explain this seemingly paradoxical role for $BRAF^{V600E}$ is oncogene-induced senescence (OIS)[9]. Cellular senescence is defined as the permanent cell-cycle arrest of previously replication-competent cells[10,11]. Senescence is associated with a variety of molecular hallmarks including elevated expression of $p16^{INK4A}$ and other cyclin-dependent-kinase inhibitors, TP53, H2AX, lysosomal beta-galactosidase and senescence-associated secretory proteins (SASP) as well as a DNA content profile indicative of arrest in the G0/G1 phases of the cell cycle[11–16]. The concept of OIS as a barrier to tumorigenesis derived from observations of a durable proliferation arrest induced by overexpression of oncogenic RAS or RAF in immortalized human fibroblasts[12,17].

More recent studies have questioned whether the term "senescence" aptly describes proliferation arrest of melanocytic nevi. Cell cycle re-entry that accompanies nevus recurrence[18], eruption[19], or transformation to primary melanoma suggests that the nevus arrest phenotype is reversible rather than permanent. Similarly, the expression of senescence markers do not readily distinguish human melanocytic nevi from primary or transformed melanocytes in humans (16^{INK4A}, TP53, H2AX and beta-galactosidase) or mice (any known hallmark of senescence)[8,20,21]. Setting aside the permanence of OIS, melanocytic nevus arrest was largely thought to be driven by induction of $p16^{INK4A}$ expression from the *CDKN2A* gene. Indeed, early studies demonstrated that $BRAF^{V600E}$ induces $p16^{INK4A}$ expression and that melanocytic nevi frequently express high levels of $p16^{INK4A}$ [9]. Despite this, $p16^{INK4A}$ expression is neither ubiquitous across melanocytic nevi, nor uniform within the cells of a single nevus[22,23], and neither knock down of the 16^{INK4A} transcript nor ablation of the *CDKN2A* locus prevents the onset or rescues $BRAF^{V600E}$-induced proliferation arrest[9,23–25]. $BRAF^{V600E}$ also stimulates expression of $p15^{INK4B}$ - the translational product of the *CDKN2B* gene[25] which is situated adjacent to the *CDKN2A* locus - suggesting $BRAF^{V600E}$ might orchestrate arrest via multiple cyclin dependent kinase inhibitors that induce arrest in the G1 phase

of the cell cycle, prior to genome synthesis. While the loss of the *CDKN2A/B* locus is a formative event in melanoma progression, genetic evolution studies of melanoma progression suggest that selection against the *CDKN2A/B* locus occurs after BRAF^{V600E} melanocytes have already escaped nevus-associated arrest[23,26]. Collectively, these data complicate the straightforward model wherein BRAF^{V600E} induces the expression of cell cycle regulators leading to proliferation arrest, which is later circumvented by the genetic loss of those regulators.

Given these observations, we reasoned that the arrest response of human melanocytes to BRAF^{V600E} might be distinct from previous reports of BRAF^{V600E}-induced OIS in other cell types. Specifically, we hypothesized that nevus-associated arrest is conditional and coordinated by reversible changes in gene expression. Here, we identify a transcriptional program that is consistently elevated in melanocytic nevi and includes microRNAs (miRNAs) previously shown to have diagnostic value[27,28]. In parallel, we observe that, unlike RAF-induced OIS in fibroblasts, BRAF^{V600E}–induced arrest in human melanocytes is reversible and conditional. Merging these two observations, we discover that in melanocytes, regulation of miRNAs coupled to differentiation status permits toggling between BRAF^{V600E}-driven hyperproliferative to arrested phenotypes.

Results

Melanocytic nevus- enriched miRNAs induce mitotic failure and proliferation arrest in primary human melanocytes

Since melanocytic nevi do not consistently express known senescence markers, we sought to characterize the transcripts that are specifically elevated within nevus melanocytes (Fig. 1A). We analyzed previously published datasets comparing RNA expression between benign and malignant melanocytic lesions[26,28]. Each clinical specimen contained matched RNA samples derived from melanocytic nevi and melanomas that arose from those nevi. We reasoned that down-regulated transcripts within these newly-formed melanomas could represent the most immediate barriers to melanocyte growth. Of the differentially expressed genes (adjusted p value <0.05), six of the top ten with elevated expression in nevi were non-coding miRNAs (Fig. 1B and Table S1). Among these were miRNAs previously shown as enriched in nevi compared to melanomas, including MIR211-5p, MIR125A-5p, MIR125B-5p and MIR328-3p[28,29]. To determine whether elevated expression of these miRNAs distinguished nevus melanocytes from normal epidermal melanocytes, we profiled melanocytes from fresh healthy skin and nevi (Table S2). Three of the miRNAs (MIR211-5p, MIR328-3p, MIR125B-5p) were also more highly expressed in melanocytic nevi as compared to healthy melanocytes or melanomas - an expression pattern consistent with enrichment in arrested melanocytes - whereas one miRNA (MIR125A-5p) presented a pattern consistent with lineage specific expression that is lost upon

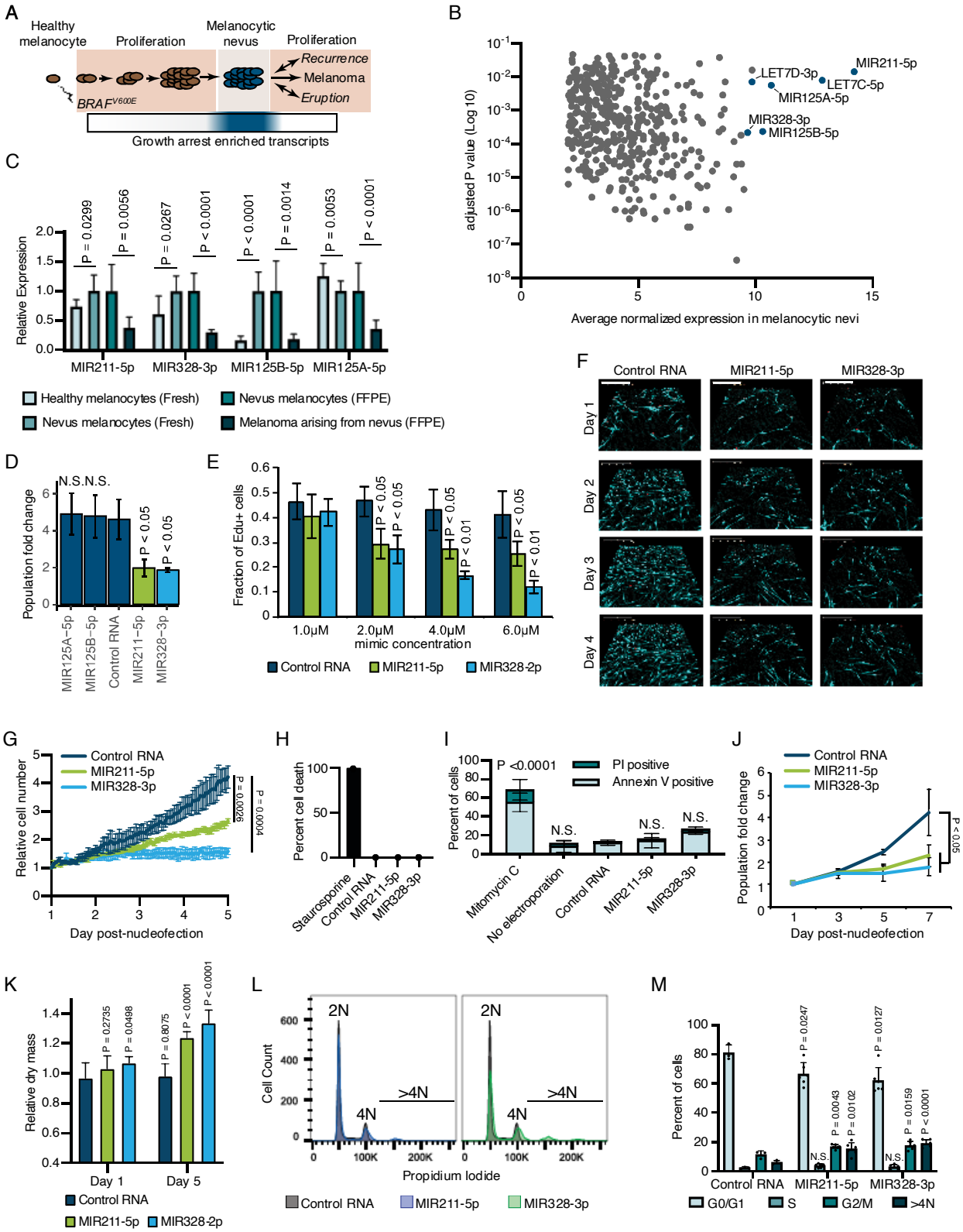
A
Healthy melanocyte
Proliferation
Melanocytic nevus
Proliferation
Recurrence
Melanoma
Eruption
BRAF V600E
Growth arrest enriched transcripts
B
adjusted P value (Log 10)
Average normalized expression in melanocytic nevi
MIR211-5p
LET7D-3p
LET7C-5p
MIR125A-5p
MIR328-3p
MIR125B-5p
C
Relative Expression
MIR211-5p
MIR328-3p
MIR125B-5p
MIR125A-5p
Healthy melanocytes (Fresh)
Nevus melanocytes (FFPE)
Nevus melanocytes (Fresh)
Melanoma arising from nevus (FFPE)
D
Population fold change
N.S.N.S.
MIR125A−5p
MIR125B−5p
Control RNA
MIR211−5p
MIR328−3p
E
Fraction of Edu+ cells
1.0μM
2.0μM
4.0μM
6.0μM
mimic concentration
Control RNA
MIR211-5p
MIR328-2p
F
Control RNA
MIR211-5p
MIR328-3p
Day 1
Day 2
Day 3
Day 4
G
Relative cell number
Control RNA
MIR211-5p
MIR328-3p
Day post-nucleofection
H
Percent cell death
Staurosporine
Control RNA
MIR211-5p
MIR328-3p
I
Percent of cells
PI positive
Annexin V positive
Mitomycin C
No electroporation
Control RNA
MIR211-5p
MIR328-3p
J
Population fold change
Control RNA
MIR211-5p
MIR328-3p
Day post-nucleofection
K
Relative dry mass
Day 1
Day 5
Control RNA
MIR211-5p
MIR328-2p
L
Cell Count
2N
4N
>4N
Propidium Iodide
Control RNA
MIR211-5p
MIR328-3p
M
Percent of cells
Control RNA
MIR211-5p
MIR328-3p
G0/G1
S
G2/M
>4N

Figure 1: Melanocytic nevus enriched miRNAs induce arrest in primary human melanocytes

(A) Schematic of hypothesized plastic nature of $BRAF^{V600E}$- and nevus- associated proliferation arrest. Expression of the predicted nevus enriched transcriptional program is highlighted in blue. **(B)** Scatter plot depicting gene expression combining publicly available sequencing datasets totaling 14 melanoma-arising-from-nevus specimens, dissected into benign and malignant portions (28 total samples). Plotted are the adjusted p values (DESeq2) comparing matched nevus and melanoma samples against average normalized expression in nevus portion. Only genes exhibiting both high expression and significant differential expression in nevus portions are plotted (see Methods). The full list of genes is included as Table S1. **(C)** Left two columns, the relative expression of indicated miRNAs in freshly isolated human melanocytes from $BRAF^{V600E}$ melanocytic nevi (n = 6) compared to $BRAF^{WT}$ healthy skin melanocytes (n = 8). Right two columns, the relative expression of indicated miRNAs in melanocytes dissected from FFPE nevus (n = 7) or melanoma (n = 7) specimens. Data represent mean and standard deviation of normalized RNA sequencing read counts relative to nevus-derived samples. **(D)** Mean and standard deviation for population fold change over seven days of melanocytes nucleofected with indicated miRNA mimics compared to non-targeting control (Control RNA) (n = 3). **(E)** Mean and standard deviation for fraction of EdU positive cells 4 days after nucleofection with indicated concentrations of miRNA mimics (n= 3). P values indicate comparisons to concentration matched control. **(F)** Representative QPI images of melanocytes nucleofected with indicated miRNA mimics. Pixel color indicates low (black), mid (blue) or high (red) optical density. Scale bar = 200μm. **(G)** Mean and standard deviation for relative QPI-derived cell number over time (n = 3). **(H)** Mean and standard deviation for QPI-derived cell death counts as percentage of total cells imaged on day 1 (n = 3). Cells treated with 0.1 μM staurosporine were included as a control (n = 1) for induction of cell death. **(I)** Mean and standard deviation for percent Annexin V/PI positive cells nucleofected with indicated miRNA mimics (n = 3). Cells treated with 5μg/ml mitomycin C were included as a control (n = 3) for induction of apoptosis. **(J)** Mean and standard deviation for relative cell number over time (n = 3). **(K)** Mean and standard deviation for relative QPI-derived dry mass per cell (n = 3). **(L)** Representative histograms of DNA content profiling via propidium iodide incorporation measured by flow cytometry 5 days post- nucleofection of miRNA mimics. **(M)** Mean and standard deviation for percent of cells in indicated phases of cell cycle based upon profiles as in (K) (n = 3-6, individual datapoints shown). P values for D-L calculated by unpaired t tests comparing experimental to Control RNA. N.S. = not significant ($P \geq 0.05$)

transformation (Fig. 1C). We conclude that MIR211-5p, MIR328-3p, MIR125B-5p are transcripts specifically enriched in arrested melanocytic nevi.

To investigate whether elevated expression of MIR211-5p, MIR328-3p, or MIR125B-5p induce melanocytic arrest, we introduced synthesized mimetics of the mature miRNAs into primary human melanocytes and tracked proliferation over seven days in culture. The introduction of either MIR211-5p or MIR328-3p resulted in significantly fewer melanocytes compared to a non-targeting control (Fig. 1D). Increased concentrations of these mimics resulted in a dose-dependent decrease in EdU uptake, consistent with a cell cycle defect (Fig. 1E). To better characterize the effect of MIR211-5p or MIR328-3p expression on cell cycle and cell viability, we performed time-lapsed quantitative phase imaging (QPI). We and others have previously established QPI as a method for adherent cell cytometry that can simultaneously measure melanocyte proliferation, cell death, and cell cycle stage with single cell resolution[30–32]. Images were taken every hour for 5 days post-nucleofection (Fig. 1F). Cells expressing MIR211-5p or MIR328-3p exhibited significantly reduced growth curves (Fig. 1G). We observed no evidence of increased cell death (Fig. 1H), and confirmed this result with Annexin V staining (Fig. 1I). Experiments performed using three additional melanocyte preparations counted over seven days post

156 nucleofection yield similar results (Fig. 1J). Thus, MIR211-5p and MIR328-3p induce proliferation arrest in
157 human melanocytes.
158
159 Further characterization of the QPI images revealed a distinct increase in intra-cellular dry mass in
160 proliferation-arrested conditions (Fig. 1K). The dry mass of a cell is a measurement of total biomass
161 (DNA, RNA, proteins, lipids, etc) and is quantitatively measured by QPI. Relative dry mass fluctuates with
162 cell cycle stage in a predictable manner[30]. The 20-40% increase we observed here is characteristic of
163 cells that have doubled their DNA content but failed to complete mitosis. We confirmed this finding by
164 measuring DNA content of the arrested populations (Fig. 1L). We observed significant increases of cells
165 with both 4N DNA content and greater than 4N DNA content, indicative of cytokinetic failure following
166 DNA replication (Fig. 1M). Consistent with this interpretation, time-lapsed imaging revealed incidences of
167 tripolar mitosis and anaphase bridging in miRNA-expression melanocytes – both processes associated
168 with cytokinetic failure[33] - which were not observed in control conditions or standard culture (Video 1 and
169 Figure 1 – figure supplement 1). We conclude that MIR211-5p and MIR328-3p induce mitotic failure and
170 proliferation arrest when introduced into primary human melanocytes.

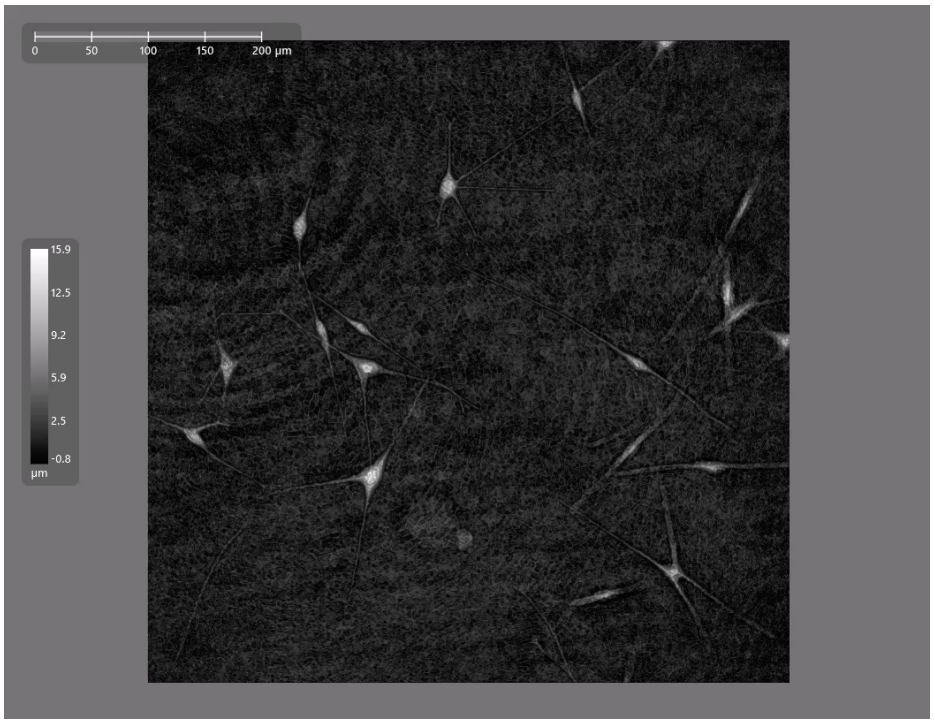

171
172 **Video 1: Cytokinesis failure associated with MIR211-5p expression.**
173 Four day time-lapse quantitative phase imaging of cytokinesis failure in primary melanocytes transduced with MIR211-5p.
174

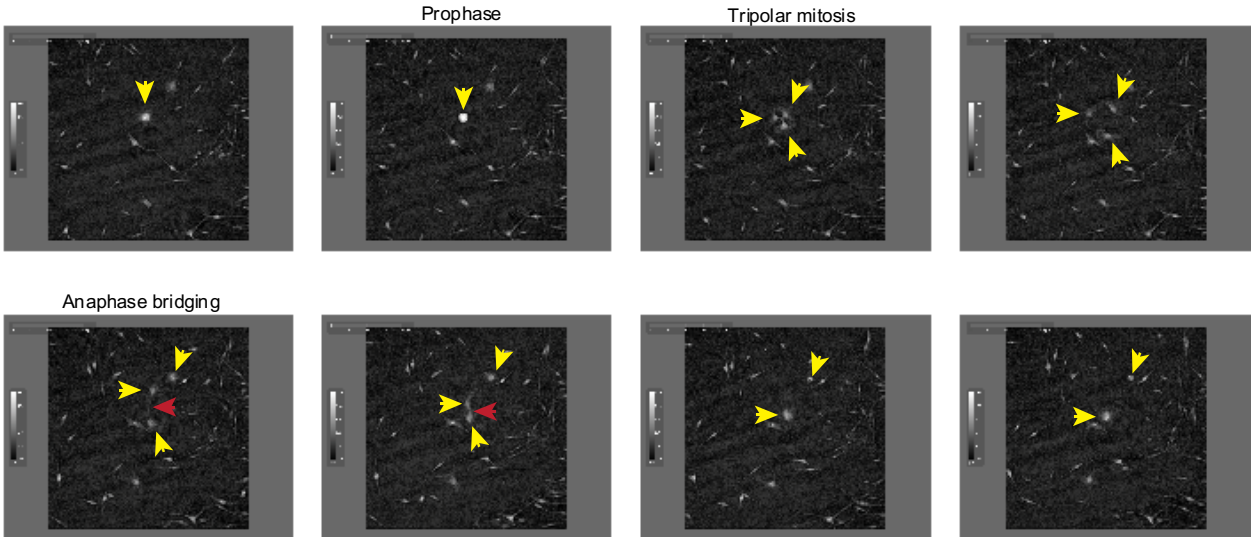

Figure 1-figure supplement 1

Still frames from Video 1 documenting representative cytokinesis failure in primary melanocytes transduced with MIR211-5p. Yellow arrow heads follow a single cell and its progeny through a tripolar mitosis. Red arrow head follows an anaphase bridge connecting two daughter cells that then remerge.

Inhibition of AURKB by MIR211-3p and MIR328-5p restricts proliferation in nevi

To investigate the mechanism by which MIR211-5p and MIR328-3p induce arrest in primary human melanocytes, we applied our previously established pipeline for identification of relevant miRNA targets (Fig. 2A)[34]. First, we nucleofected MIR211-5p, MIR328-3p, or control RNA mimics into primary human melanocytes freshly isolated from four independent donors and conducted RNA sequencing (Table S3). We next selected all genes that were significantly downregulated by either miRNA as compared to the control RNA, and further refined the set to the computationally predicted targets of MIR211-5p and/or MIR328-3p. Finally, we nucleofected siRNAs targeting the 115 resulting genes and assayed for reduced EdU incorporation that would phenocopy MIR211-5p or MIR328-3p expression (Table S4). As expected, computationally predicted targets of MIR211-5p and MIR328-3p were enriched in the set of downregulated genes following MIR211-5p or MIR328-3p nucleofection, respectively (Fig. 2B). AURKB, GPR3, and MAPKAPK2 showed the greatest magnitude of repression due to miRNA expression with significant EdU reduction upon siRNA-mediated knockdown (Fig. 2C). Of these, AURKB (predicted MIR211-5p target) and GPR3 (predicted MIR328-3p target), were significantly inhibited upon nucleofection of either miRNA (Fig. 2D). We reasoned these genes might represent convergent nodes driving proliferation arrest. Further exploration of the AURKB transcript revealed a potential MIR328-3p binding site just before the 3' untranslated region (Fig. 2E). In contrast, we were unable to identify a candidate MIR211-5p binding site in the GPR3 transcript, suggesting indirect inhibition of this gene by MIR211-5p.

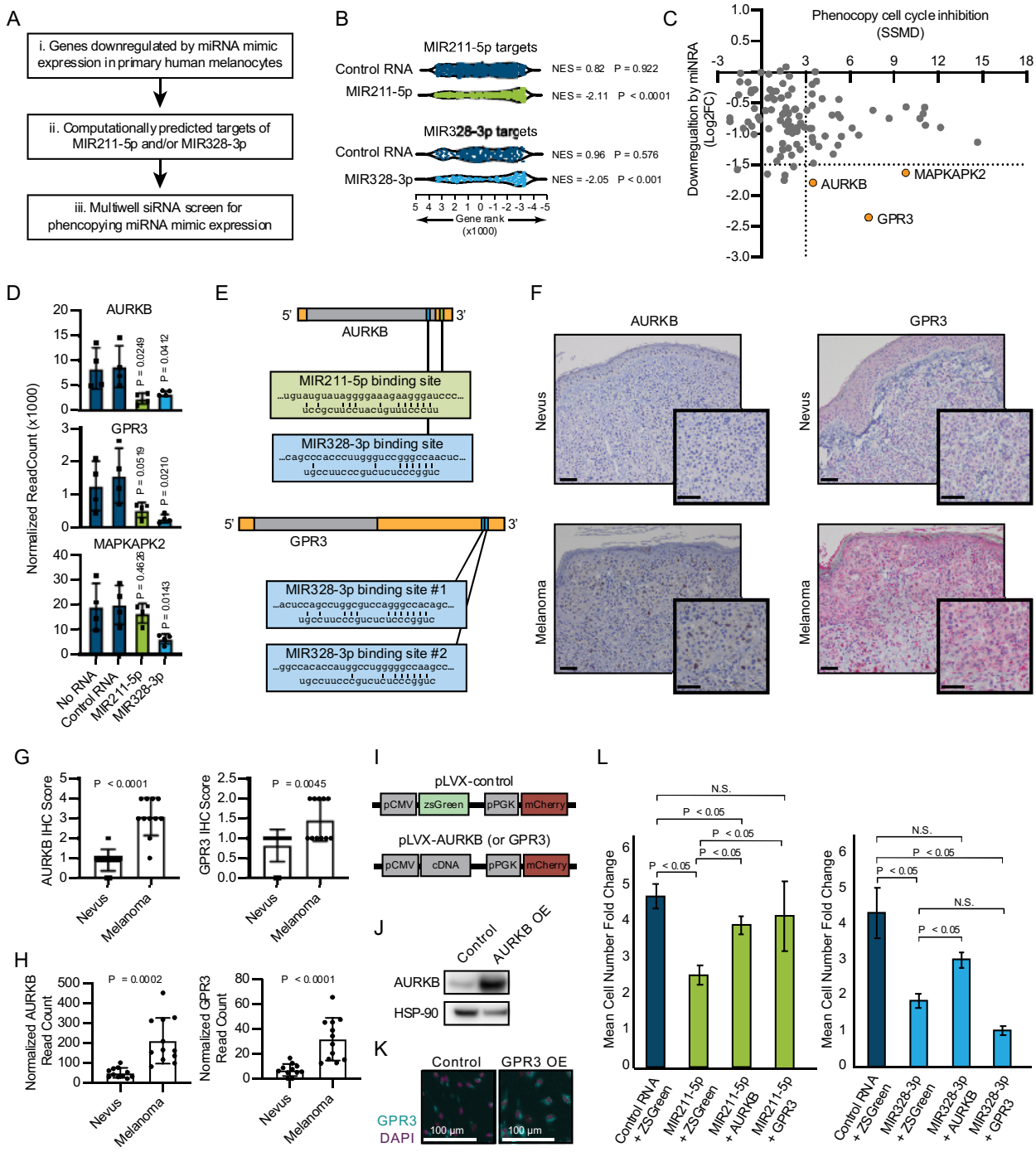

Figure 2: Inhibition of AURKB by MIR211-3p and MIR328-5p restricts proliferation in nevi

(A) Schematic of experimental and computational pipeline for identifying targets of MIR211-3p and/or MIR328-3p responsible for proliferation arrest. **(B)** GSEA analysis comparing predicted MIR211-5p and MIR328-3p target mRNAs to changes in gene expression after nucleofection with indicated mimics compared to nucleofection control. NES = normalized enrichment score. P = nominal P value. Table S3 provides full differentially expressed gene lists. **(C)** Plot of siRNA screen results for phenocopying proliferation arrest versus log2 fold change in expression after miRNA mimic nucleofection. Strictly

standardized mean difference (SSMD) reports the magnitude and significance of inhibition of Edu incorporation (n = 3, see Table S4 for list of genes and screen results). Dotted lines indicate cut-off values for further evaluation. Orange points indicate genes meeting cut-off criteria. **(D)** Mean and standard deviation for expression of indicated genes after nucleofection of indicated mimics (n = 4). P values calculated by unpaired t tests compared to No RNA. **(E)** Schematics showing predicted binding sites of MIR211-5p and MIR328-3p in AURKB and GPR3 transcripts. **(F)** Representative images of immunohistochemical staining for AURKB (brown chromagen) and GPR3 (red chromagen) expression in FFPE samples of nevi and melanoma. Scale bars = 50μm. **(G)** Mean and standard deviation for immunohistochemical staining scores as in (F) for cohorts of 11 nevi and 11 melanomas. P values calculated by unpaired t tests. **(H)** Mean and standard deviation for read counts for cohorts of 11 nevi and 12 melanomas. P values calculated by unpaired t tests. **(I)** Design of pLVX vectors expressing either AURKB or GPR3. **(J)** Western Blot of AURKB expression in human melanocytes with or without lentiviral AURKB overexpression. HSP90 is the loading control. Source data provided as supplemental files (Fig_2_J_Source). **(K)** Representative photomicrographs (20X) of immunofluorescence for GPR3 (green) or (DAPI) (purple) in human melanocytes with GPR3 lentiviral overexpression (GPR3 OE) or without (Control) over-expression. **(L)** Mean and standard deviation for cell number fold change over 7 days after nucleofection with indicated miRNA mimics in melanocytes transduced with lentiviral constructs expressing zsGreen, AURKB, or GPR3 (n = 6 melanocyte preps, type 2 t test, N.S. = not significant (P ≥ 0.05)). P values calculated by unpaired t tests.

To determine whether decreased AURKB and/or GPR3 expression was associated with melanocytic nevi, we acquired 23 clinical specimens and measured both the transcript and protein expression of these genes (Fig. 2F-H). The expression of both AURKB and GPR3 protein and mRNA were enriched in melanomas as compared to nevi (Fig. 2G-H). Together, these data demonstrate an inverse expression between two miRNAs (MIR211-5p and MIR328-3p) and two targeted mRNAs (AURKB and GPR3) that toggles concurrently with the transition of arrested melanocytic nevi to melanomas. To further investigate whether either mRNA was sufficient to rescue miRNA-mediated arrest, primary melanocytes were transduced with constructs expressing either zsGreen (control), AURKB or GPR3 (Fig. 1I-K) then subsequently nucleofected with either MIR211-5p or MIR328-3p. Expression of either mRNA partially rescued MIR211-5p-induced arrest, while AURKB, but not GPR3, partially rescued MIR328-3p-induced arrest (Fig. 2L). Thus, while other MIR211-5p and MIR328-3p targets, including GPR3, may play a role in the induction of melanocyte proliferation arrest, these data suggest that AURKB inhibition is a critical convergent node of both miRNAs in facilitating proliferation arrest in nevi. This interpretation is further supported by the well-established role of AURKB as an essential orchestrator of successful mitosis[35].

BRAF^{V600E} induces a reversible and conditional proliferation arrest in human melanocytes

We hypothesized that AURKB inhibition by MIR211-5p and MIR328-3p may be the underlying mechanism by which BRAF^{V600E} induces proliferation arrest in melanocytes. BRAF^{V600E} expression has been demonstrated to result in an accumulation of growth-arrested fibroblasts with 2N DNA content, presumably in a permanent G0/G1 senescent state[9,12,17]. In contrast, upon overexpression of MIR211-5p or MIR328-3p, we observed an accumulation of arrested melanocytes with ≥4N DNA content, and a significant decrease in cells with 2N DNA content (Fig. 1M). To determine the DNA content profile of primary human melanocytes under BRAF^{V600E}-induced arrest, we utilized an established lentiviral construct for dose-responsive doxycycline inducible BRAF^{V600E} expression (Fig. 3A)[25]. We monitored

melanocyte growth under a titration of doxycycline and identified the lowest concentration (15.6 ng/mL) that induced sustained arrest after 40 hours exposure (Fig. 3B). Similar to our observations for miRNA-induced arrest, relative per cell dry mass increased by 50% concurrent with BRAF^{V600E} induced- arrest (Fig. 3C). Cell cycle profiling confirmed a significant and dose-dependent accumulation of cells with ≥4N

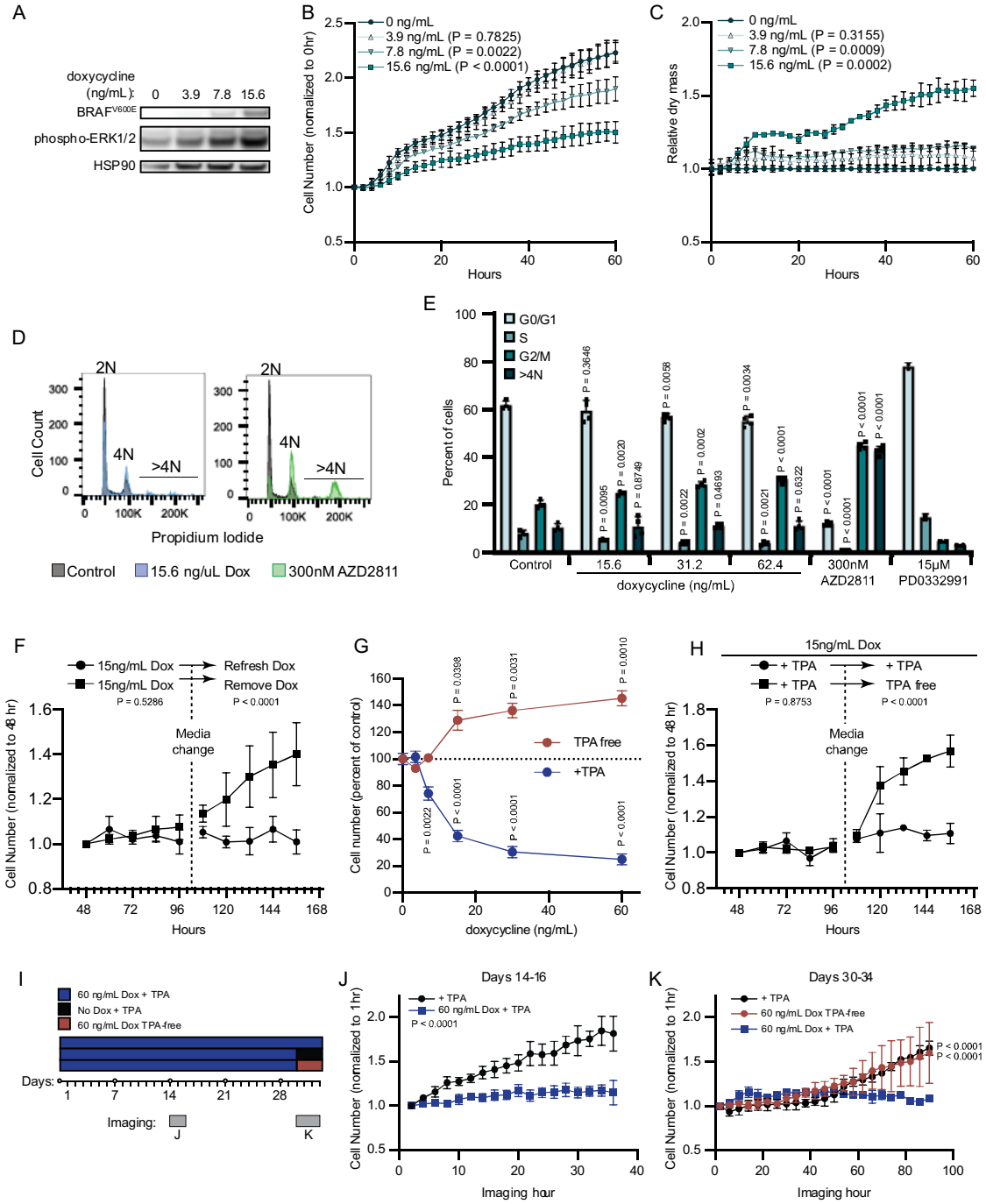

Figure 3: BRAF^{V600E} induces a reversible and conditional arrest in human melanocytes

(A) Representative (of n = 3) Western Blot analysis of BRAF^{V600E}, phospho-ERK1/2, and HSP90 (loading control) in diBRAF^{V600E} melanocytes in response to increasing concentration of doxycycline. Source data provided in supplemental files (Fig_3A_Source). **(B)** Mean and standard deviation for relative QPI-derived cell number at indicated hours of

diBRAF^{V600E} melanocytes in response to increasing concentration of doxycycline (n = 6). P values from unpaired t tests comparing to 0 ng/mL condition. **(C)** Mean and standard deviation for relative QPI-derived dry mass per cell of diBRAF^{V600E} melanocytes in response to increasing concentration of doxycycline at indicated hours (n = 6). P values from unpaired t tests comparing to 0 ng/mL condition. **(D)** Representative histograms of DNA content profiling via propidium iodide incorporation measured by flow cytometry 5 days after treatment with indicated molecules. AZD2811 included as a control for induced cytokinesis failure. **(E)** Mean and standard deviation for percent of cells in indicated phases of cell cycle after treatment with doxycycline based upon profiles as in (D) (n = 4). AZD2811 (n = 4) is a control for induced cytokinesis failure. PD0332991 (n = 2) is a control for G0/G1 arrest. P values from unpaired t tests comparing to Control (no treatment) condition. **(F)** Mean and standard deviation for relative QPI-derived cell number of diBRAF^{V600E} melanocytes at indicated hours after treatment doxycycline. Dotted line indicates change in media to either refresh doxycycline or add media without doxycycline (n = 3). P values from unpaired t tests comparing final timepoints. **(G)** Mean and standard deviation for cell number as percent of control of diBRAF^{V600E} melanocytes cultured with or without TPA after 5 days of treatment with indicated concentrations of doxycycline. P values from unpaired t tests comparing to 0 ng/mL conditions. Baseline population doubling times were 3.2 days (+TPA) and 4.2 days (TPA-free). **(H)** Mean and standard deviation for relative QPI-derived cell number of diBRAF^{V600E} melanocytes at indicated hours after treatment doxycycline. Dotted line indicates change in media to either refresh TPA-containing media or add media without TPA (n = 3). P values from unpaired t tests comparing final timepoints. **(I)** Schematic of experimental design testing the reversibility of growth arrest after 30 days exposure to high doxycycline (60 ng/mL). Days of live imaging represented in (J) and (K) are indicated by grey bars. **(J)** Mean and standard deviation for relative QPI-derived cell number of diBRAF^{V600E} melanocytes at 14 days after addition of doxycycline (n = 3). P values from unpaired t tests comparing final timepoints. **(K)** Mean and standard deviation for relative QPI-derived cell number of diBRAF^{V600E} melanocytes at 30 days after addition of doxycycline (n = 3). Media was changed just prior to imaging to either refresh doxycycline (blue), +TPA media without doxycycline (black) or add TPA-free media with doxycycline (red). P values from unpaired t tests comparing final timepoints.

DNA content and a decrease in cells with 2N DNA content (Fig. 3D-E). The cell cycle profiles were notably dissimilar to that of melanocytes treated with a pharmacologic CDK4/6 inhibitor (PD0332991, Palbociclib)[36] known to induce G0/G1 arrest. Treatment with a pharmacologic AURKB inhibitor (AZD2811, Barasertib)[37] that induces G2/M arrest and mitotic failure also resulted in an accumulation of melanocytes with ≥4N DNA content and a decrease in cells with 2N DNA content.

In addition to the accumulation of 2N cells, previous reports of RAF expression in fibroblasts show that transient expression can induce a durable arrest phenotype[17]. To test the durability of BRAF^{V600E}-induced arrest in human melanocytes, we induced doxycycline-dependent BRAF^{V600E} expression for 48 hours and monitored cell number for an additional two days to confirm arrest. Media was then replaced to remove doxycycline. Within twelve hours of doxycycline removal, the previously arrested melanocytes began to proliferate (Fig. 3F), demonstrating that BRAF^{V600E}-induced proliferation arrest in melanocytes is reversible and dependent on continued oncogene expression.

Nevi recurrence after excision[18] and eruption upon external stimuli[19], together with our observation that BRAF^{V600E} induced arrest is reversible in melanocytes, suggested that BRAF^{V600E}-induced arrest may depend on secondary signals from the microenvironment. Tetradecanoylphorbol acetate (TPA) is a protein kinase C (PKC) activator commonly used as a mitogen in primary melanocyte media to substitute

303 for endothelin receptor type B activation[38]. In contrast, TPA also inhibits the cell cycle of melanoma
304 cells[39,40]. BRAF^{V600E} expression permits growth of the Melan-A cell line in the absence of TPA[41]. We
305 therefore wanted to determine the relative contributions of TPA and BRAF^{V600E} to the BRAF^{V600E}-induced
306 primary melanocyte arrest *in vitro*. We induced BRAF^{V600E} expression in primary human melanocytes in
307 two medias – one containing TPA (+TPA) or one containing the endothelin receptor type B ligand,
308 endothelin-1 (TPA-free) and observed divergent dose-responsive phenotypes (Fig. 3G). In the presence
309 of TPA, BRAF^{V600E} expression inhibited cell proliferation. By contrast, in TPA-free media, BRAF^{V600E}
310 expression induced proliferation. We next subjected melanocytes to the arrest-inducing conditions of
311 doxycycline treatment in +TPA media for four days, then replaced with doxycycline-containing, TPA-free
312 media. We observed a rapid shift to the proliferative phenotype even in the continued presence of
313 doxycycline (Fig. 3H). To determine whether the observed reversibility of BRAF^{V600E}-induced growth
314 arrest was due to insufficient duration or degree of expression of the oncogene, we exposed melanocytes
315 to a high concentration of doxycycline (60ng/mL) for 30 days prior to switching medias (Fig. 3I).
316 Melanocytes in +TPA media remained arrested for the duration of doxycycline treatment then grew
317 readily upon removal of either doxycycline or TPA (Fig. 3J-K). From these results, we conclude that
318 BRAF^{V600E} expression induces divergent and interconvertible phenotypes – either hyperproliferation or a
319 reversible arrest – in human melanocytes conditional on extrinsic stimuli.
320
321 **BRAF^{V600E}-induced arrest is dependent on melanocyte growth conditions and differentiation state**
322 To investigate the relative contributions of BRAF^{V600E} and TPA to the expression of MIR211-5p and
323 MIR328-3p, we conducted small RNA sequencing of melanocytes grown in +TPA or TPA-free media and
324 with or without BRAF^{V600E} expression. The expression of MIR328-3p was relatively stable, demonstrating
325 less then 2-fold changes across conditions (Fig. 4A-B, Table S5). In contrast, MIR211-5p was one of the
326 most differentially expressed genes in +TPA conditions compared to TPA-free conditions (adj. P = 6.8E-
327 23) (Fig. 4A-B, Table S5). Induction of BRAF^{V600E} in +TPA conditions did not further alter expression of
328 either miRNA. Direct comparison of the arrested melanocytes in +TPA +Dox conditions to the proliferative
329 melanocytes in -TPA +Dox conditions revealed MIR211-5p as the most significantly downregulated
330 miRNA in the proliferative condition (Fig. 4B). Thus, in comparison to TPA, BRAF^{V600E} induction had
331 minimal effect on the expression of the miRNAs. The most notable effect was a decrease of MIR328-3p
332 expression coinciding with the induction of BRAF^{V600E} in TPA free conditions (Fig. 4A). While MIR328-3p
333 downregulation likely contributes to increased proliferation in this condition, the more pronounced effect of
334 TPA on MIR211-5p expression suggests that the mechanisms governing whether BRAF^{V600E} induces
335 arrest or proliferation are a function of the cell's transcriptional state rather than directly downstream of
336 BRAF^{V600E} itself.
337
338 To better characterize the two transcriptional states influencing the BRAF^{V600E} phenotype, we conducted
339 mRNA sequencing of the same specimens. Principal component (PC) analysis revealed that 97.4% of the

variance between samples was explained by two principal components – PC1 (81.7% variance) separated transcriptomes based upon exposure to TPA and PC2 (15.7% variance) separated transcriptomes based upon BRAF^{V600E} expression (Fig. 4C, Table S5). We conducted differential expression analyses to compare all samples exposed to +TPA versus TPA-free media, regardless of BRAF^{V600E} expression (Fig. 4D, top) and to compare all samples expressing BRAF^{V600E}, regardless of TPA exposure (Fig. 4D, bottom). As expected from the PC analysis and similar to the miRNA profiles, most gene expression variance was due to media conditions with a smaller, but consistent, set of genes activated by BRAF^{V600E}.

One initially surprising result of this analysis was the static expression of both MIR211-5p and MIR328-3p in +TPA conditions, regardless of BRAF^{V600E} expression. However, as inhibitors of translation, miRNA function depends on the expression level of its targets[42,43], effectively functioning as buffers of gene expression that prevent aberrantly high levels of a transcript[44]. BRAF^{V600E} has been previously demonstrated as an upstream activator of AURKB transcription in melanoma cells[45]. We therefore reasoned that MIR211-5p expression in +TPA conditions might dampen AURKB activation by BRAF^{V600E}. Consistent with this hypothesis, the addition of doxycycline induced AURKB expression in TPA-free / MIR211-5p low conditions, but this effect was not observed in +TPA / MIR211-5p high conditions (Fig. 4E).

We next conducted gene set enrichment analyses (GSEA) comparing TPA-regulated genes and BRAF^{V600E}- regulated genes to Molecular Signature Database Hallmark gene sets[46]., the KEGG PATHWAY database[47], and signatures important in BRAF^{V600E} signaling[48], human melanocyte differentiation[49] or melanoma cell state[50–52]. Among the pathways uniquely enriched with BRAF^{V600E} expression were the expected increases in signatures downstream of BRAF^{V600E}, MAPK (KRAS) signaling, and glycolysis[53] (Fig. 4F and Table S6). Gene sets uniquely enriched in +TPA media included signatures associated with cell cycle regulation, such as the G2-M checkpoint, oxidative phosphorylation, the MITF program, and differentiated melanocytes. In contrast, TPA-free media induced gene sets associated with cell adhesion and melanocyte progenitor and stem cells. Corroborating this observation, melanocytes grown in TPA-free media expressed higher levels of AXL (Fig. 4G-H), lower levels of MLANA, a melanocyte differentiation marker and presented greater activity of aldehyde dehydrogenase, enzymatic activity associated with stemness (Fig. 4I). These results indicate that exposure to TPA induces a more differentiated melanocyte phenotype, consistent with previous reports[54–56].

To look for synergist effects of both BRAF^{V600E} expression and media conditions, we performed pair-wise differential expression analyses of each condition (Table S6 and summarized in Figure 4-figure supplement 1). Generally, most gene sets identified in Figure 4F were regulated by only one of the two stimuli. For example, genes downstream of BRAF^{V600E} signaling were only influenced by doxycycline

377 exposure. Interesting exceptions to this trend were the inflammatory response, which required both
378 stimuli; cell cycle regulation gene sets, which were activated by TPA alone but further elevated when
379 supplemented with doxycycline; and epithelial to mesenchymal transition genes, which were activated by
380 either stimulus. A subset of melanocyte dedifferentiation gene sets, specifically neural crest genes, the
381 melanoma invasion program and the AXL program, but not markers of melanocyte stem cells, were
382 activated by either TPA-free media or $BRAF^{V600E}$ expression, albeit the activation was more pronounced
383 in the former. This observation suggests that $BRAF^{V600E}$ expression alone does induce some programs
384 associated with melanocyte dedifferentiation, but with the retention of MIR211-5p expression, the
385 induction is insufficient to overcome growth arrest.
386
387 Collectively, our transcriptomic analyses support a model whereby growth in +TPA conditions induces a
388 more differentiated state in melanocytes coinciding with an increase in MIR211-5p expression (Fig. 4J).
389 This increased MIR211-5p combined with relatively stable MIR328-3p expression, dampens entry into
390 mitosis and/or successful completion of mitosis at least in part through AURKB inhibition. The attenuation
391 of cell division results in an accumulation of cells in G2/M – an effect that is more pronounced in
392 conditions stimulating accelerated growth, such as with $BRAF^{V600E}$ expression. To test this model, we
393 transduced doxycycline-inducible $BRAF^{V600E}$ melanocytes in +TPA conditions with lentiviral constructs
394 constitutively expressing either AURKB (Fig. 2I-J) or miRNA sponges (Fig. 4K) to either MIR211-5p or
395 MIR328-3p. AURKB expression had no baseline effect on melanocyte growth, but rescued $BRAF^{V600E}$-
396 induced arrest (Fig. 4L), suggesting the inability of the oncogene to induce AURKB in this context serves
397 as a bottleneck in cell division. Also consistent with the model, sponges against either MIR211-5p or
398 MIR328-3p increased baseline division rate and rescued $BRAF^{V600E}$-induced arrest, demonstrating that
399 both miRNAs contribute to inhibition of melanocyte division, with affects that are more pronounced in the
400 presence of growth signals.
401

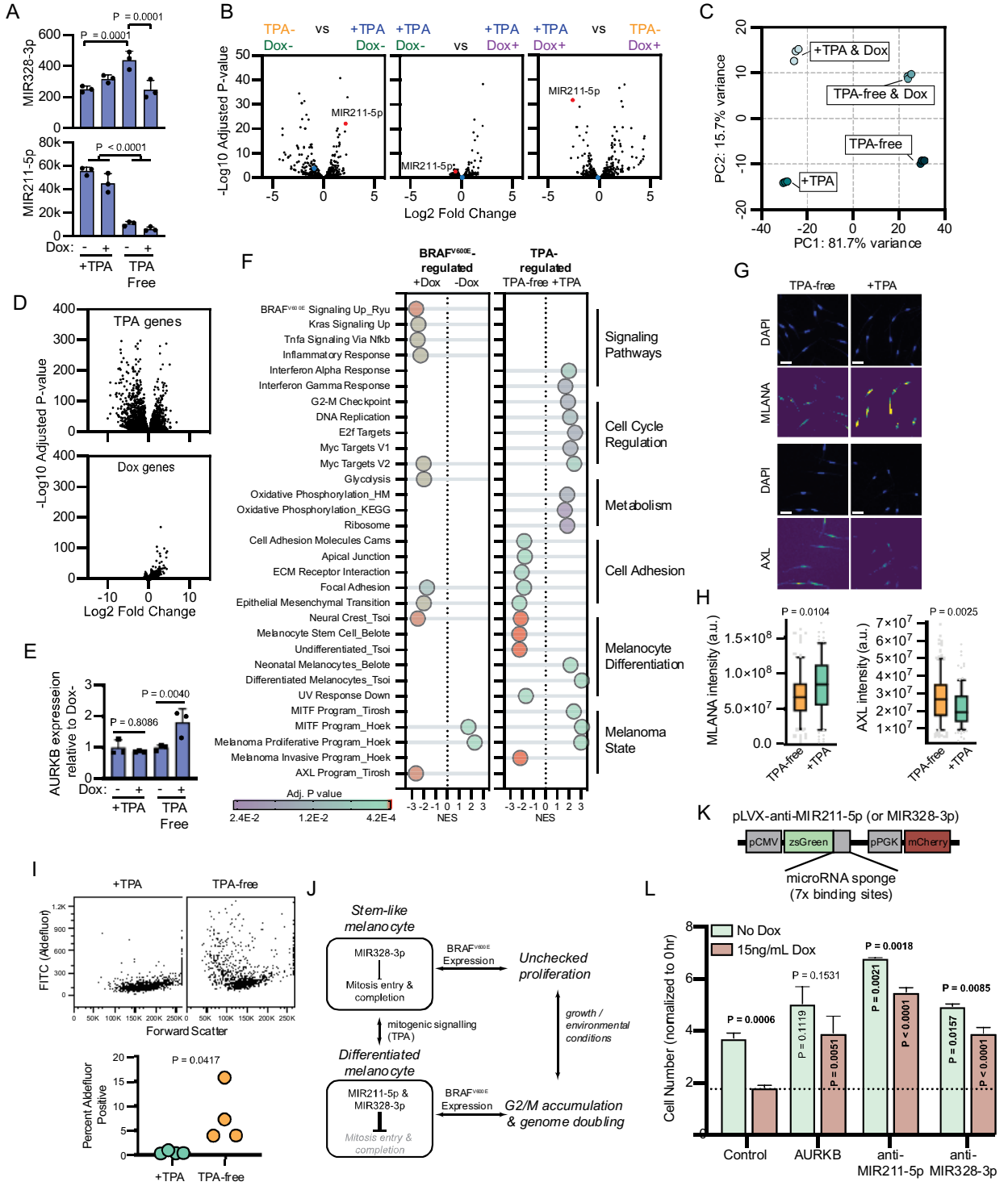

Figure 4: BRAF^{V600E}-induced arrest is dependent on melanocyte growth conditions and differentiation state

(A) Normalized read counts for MIR328-3p (top) and MIR211-5p (bottom) in TPA-containing (+TPA) or TPA-free media, with or without 15.6 ng/mL doxycycline (Dox). See Table S5 for individual values and exact P values. **(B)** Volcano plots depicting log2 fold change against adjusted P value (-Log10) from differential expression (DE) analysis of small RNA sequencing of indicated comparisons. MIR211-5p labelled and shown in red. MIR328-3p shown in blue. **(C)** First and second

principal components (PC) separating diBRAF^{V600E} melanocytes cultured in indicated conditions. **(D)** Volcano plots depicting log2 fold change against adjusted P value (-Log10) from differential expression (DE) analysis of mRNA sequencing of all +TPA specimens versus all TPA-free specimens (top) or all Dox specimens versus all no-Dox specimens (bottom). **(E)** Normalized read counts for AURKB normalized to no Dox conditions (n = 3). P values from unpaired t tests. Sequencing data represented in A-F are from n=3 per condition analyzed with DESeq2. **(F)** Gene set enrichment analysis (GSEA) comparing DE gene sets from (D) to Molecular Signature Database Hallmark gene sets, KEGG Pathway gene sets and published signatures of melanocyte signaling and differentiation from Belote, 2021; Tsoi, 2018; Tirosh, 2016; Ryu, 2011; and Hoek, 2010. All enrichments with adjusted P value < 0.025 are depicted. See Table S6 for all associations. Normalized enrichment score (NES). Enrichment differences between pathways across the four conditions in (C) are depicted in Figure 4-figure supplement 1. **(G)** Representative photomicrographs of immunofluorescence for MLANA or AXL in human melanocytes cultured in +TPA or TPA-free conditions. White scale bar = 30μm. **(H)** Quantification of fluorescence intensity (arbitrary pixel intensity units, a.u.) from experiments represented in (G). Box (median, 25th and 75th percentiles) and whiskers (10th and 90th percentiles) of 84, 88, 113, and 96 cells respectively. P values from unpaired t tests. **(I)** Representative plots (top) and quantification (bottom, n = 4) of relative aldehyde dehydrogenase activity of melanocytes grown in +TPA or TPA-free conditions. **(J)** Schematic of model supported by transcriptomic analyses. TPA induces a more differentiated state in human melanocytes. Due to increased MIR211-5p and base-line MIR328-3p expression, AURKB expression is capped, resulting in G2/M accumulation upon BRAF^{V600E} expression. **(K)** Design of pLVX vectors expressing microRNA sponges fused to zsGreen. **(L)** Mean and standard deviation for cell number as percent of time point 0 hr after 7 days of culture in +TPA media with or without 15.6 ng/mL Dox (n = 3 per condition). Melanocytes were transduced with either pLVX-control, -AURKB, -anti-MIR211-5p, or -anti-MIR328-3p. P values from unpaired t tests comparing to matched no Dox condition (horizontal), Control no Dox condition (vertical in green bar) or Control Dox condition (vertical in red bar).

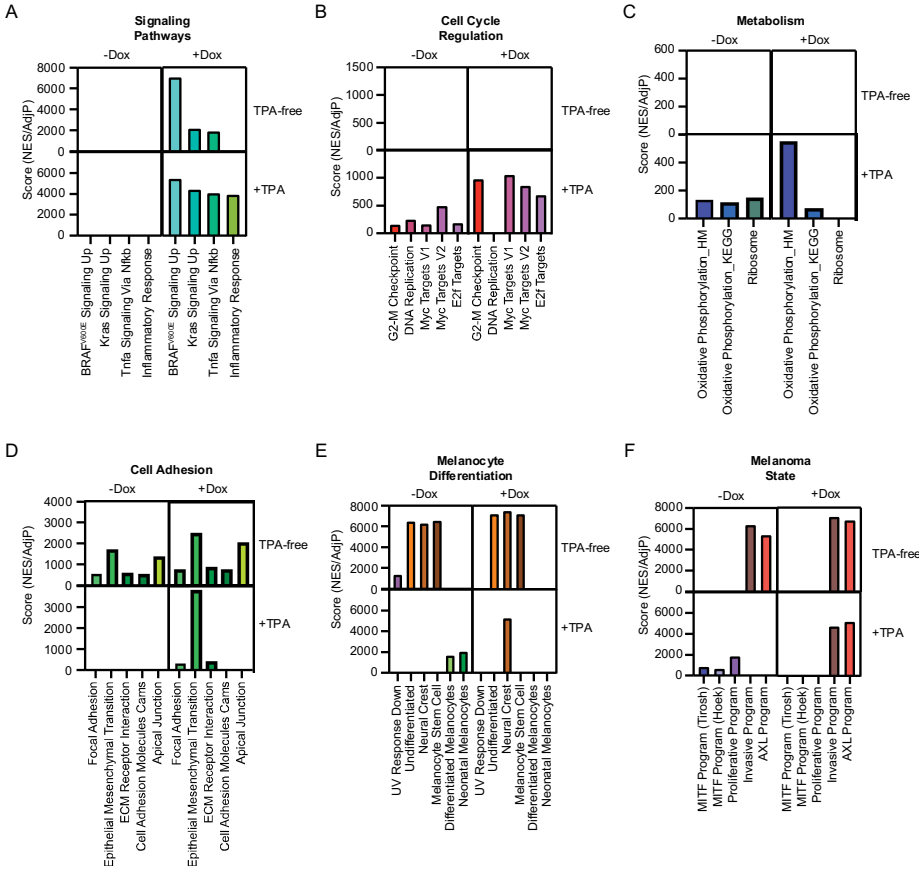

432 **Figure 4 - figure supplement 1**
433 Depiction of gene set enrichment for gene sets in Figure 1F across the four conditions in Figure 4C. Pair-wise comparisons
434 were conducted as in Figure 1F, comparing the +TPA -Dox condition to other conditions. Scores were generated by dividing
435 positive NES values by the AdjP value. For the +TPA -Dox quadrant, scores were averaged when occurring in more than
436 one pair-wise comparison.
437
438 **AURKB inhibition drives melanocytic nevus-associated proliferation arrest**
439 To further investigate whether this mechanism of arrest occurs in clinical nevus specimens, we examined
440 an independent cohort of 15 nevi for evidence of mitotic failure. Histopathologic analysis revealed that all
441 nevi within the cohort exhibited binucleation (Fig. 5A). The percent observed binucleated melanocytes
442 ranged from 3-12% (mean = 6.3%). It is important to note that since binucleation can only be observed in
443 the fraction of cells sectioned perpendicular to the plane of the adjacent nuclei, 3-12% is likely an under-
444 estimate. We also observed giant multinucleated cells in 10 of the 15 nevi, indicative of multiple rounds of
445 DNA synthesis and cytokinetic failure and consistent with previous reports[57].
446
447 We sought to determine whether AURKB inhibition was necessary and sufficient for the multi-nucleated
448 arrest we observed in melanocytic nevi. We obtained three fresh skin biopsies containing nevi,
449 microdissected the nevus portion, and isolated melanocytes (Fig. 5B). Nevus-derived melanocytes
450 appeared healthy in culture. Consistent with the histopathologic cohort, co-staining with melanocyte
451 marker, MLANA, and Hoechst revealed frequent 4N and 8N melanocytes (Fig. 5C). Transduction of
452 nevus melanocytes with an AURKB and mCherry expressing lentiviral vector at low multiplicity of infection
453 (MOI) showed that the mCherry positive cells divided significantly more than the their mCherry negative
454 counterparts (Fig. 5D-E) in cells from all three nevus donors. This result suggests that expression of
455 AURKB is also rate limiting for the proliferation of human nevus melanocytes, as we observed in primary
456 melanocytes expressing $BRAF^{V600E}$.
457
458 To test the sufficiency of AURKB inhibition to limit $BRAF^{V600E}$ hyperproliferation in melanoma, we
459 assessed normalized growth rate inhibition of three cultures - primary human melanocytes, an
460 established $BRAF^{V600E}$ human melanoma cell line, and a short-term $BRAF^{V600E}$ human melanoma culture
461 - when exposed to a pharmacologic AURKB inhibitor (Barasertib). Normalized growth rate measurements
462 (such as GR_{50}) are independent of baseline cell division rate and are demonstrably more reproducible
463 than the commonly calculated half maximal inhibitor concentration (IC_{50}) when comparing different cell
464 cultures[58]. An additional advantage of GR_{50} is the ability to distinguish growth rate inhibition (GR_{50}
465 approaches 0) versus cell death (GR_{50} is negative). Since GR_{50} calculations require proliferation curves,

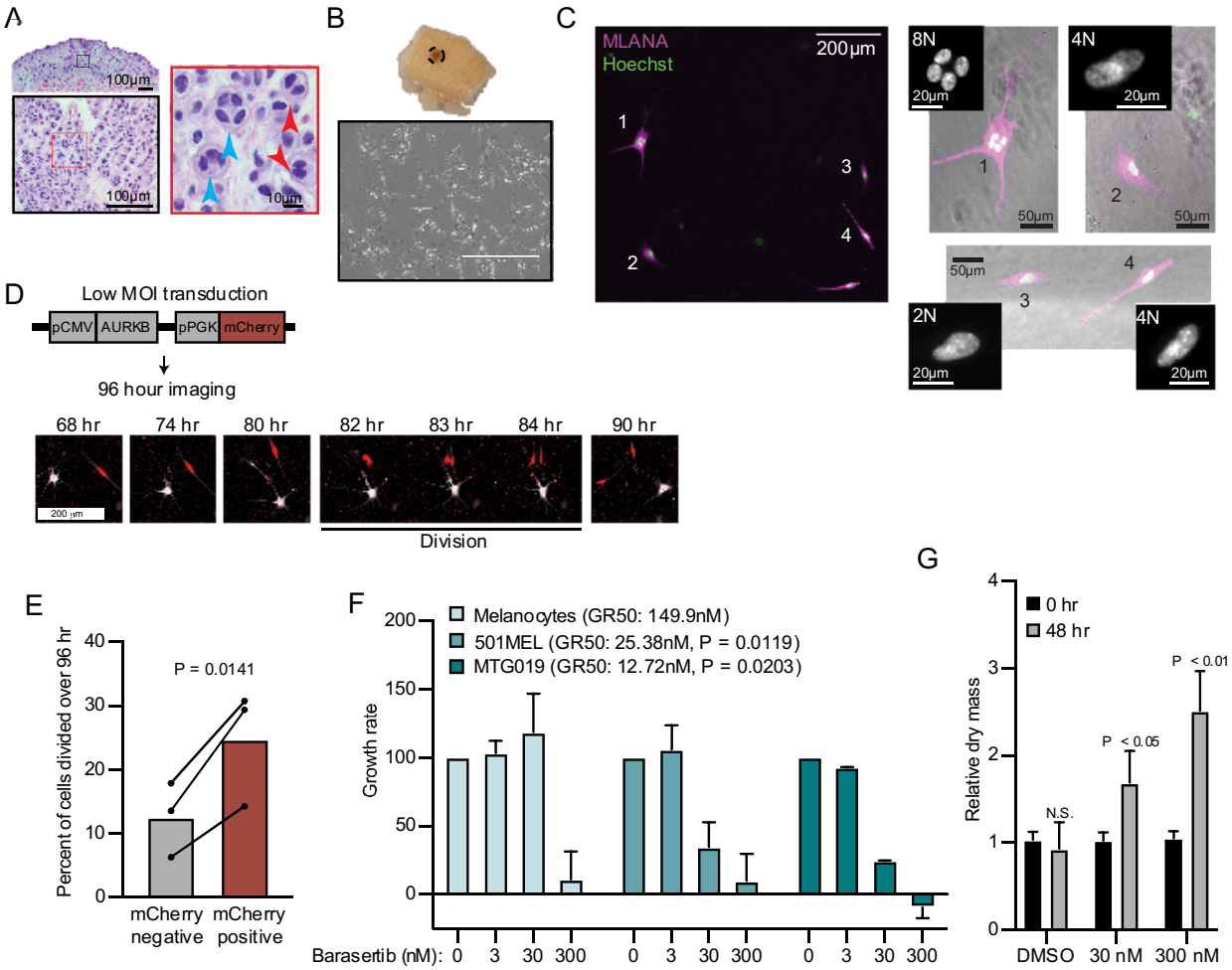

Figure 5: AURKB inhibition is critical for BRAF^{V600E}-induced arrest of human nevi

(A) Representative image of 15 H&E-stained melanocytic nevus. Border colors indicate two consecutive magnifications. Arrowheads indicate bi- (red) or multi- (blue) nucleation. **(B)** Example images of skin specimen containing a melanocytic nevus (circled) and phase contrast microscopy of melanocytes isolated from nevus portion. Scale bar = 400µm. **(C)** Images of MLANA (purple) and Hoeschst (green) co-staining of melanocytic nevus derived melanocytes in culture. Zoomed images show representative 2N, 4N, and 8N cells. **(D)** Representative of images of QPI coupled with fluorescence microscopy to identify adjacent mCherry -expressing and mCherry-negative melanocytes. Individual cells were identified at time zero, tracked and monitored for division for 96 hrs. **(E)** Mean and individual matched datapoints for the percent of n = 3 mCherry-negative or mCherry-positive cells identified at time zero that divided over 96 hrs. P value from paired t test. **(F)** Mean and standard deviation for 48 hr growth rates of indicated cells treated with Barasertib. P values from unpaired t tests comparing the 30nM samples of melanoma lines to primary melanocytes (n = 3). **(G)** Mean and standard deviation for relative QPI-derived dry mass per 501MEL cell at initial time point (black) compared to 48 hr treatment with Barasertib (grey) (n = 3). P values from unpaired t tests.

we conducted live QPI over 48 hours with a range of Barasertib concentrations (0-300nM). Primary melanocytes were largely resistant to the compound with reduced growth apparent only at supraphysiological levels (Fig. 5F). In contrast, both melanoma cultures responded to ten-fold lower dosage of the compound with GR_{50} approaching zero, indicating primarily arrest, not death. In these

conditions, the per cell dry mass also increased significantly, consistent with a G2/M arrest (Fig. 5G). Taken together, these data demonstrate that AURKB inhibition limits the rate of BRAF^{V600E}-induced proliferation in human melanocytic nevi and melanomas.

Discussion

Cellular senescence is conventionally defined as a permanent cell-cycle arrest associated with a variety of molecular markers and an irreversible arrest in the G0/G1 phase of the cell cycle[10–12]. The vast majority of melanocytic nevi are stably arrested and harbor BRAF^{V600E}, an oncogenic mutation that induces cellular senescence when expressed in a variety of mammalian cells[9,12,17]. While these observations seemingly implicate OIS as the mechanism driving nevus- associated proliferation arrest, a substantial body of evidence has challenged this paradigm in recent years[8,9,18–25]. Here, we provide further evidence to challenge the model that acquisition of BRAF^{V600E} induces premature cellular senescence in melanocytes and uncover an alternative mechanism driving nevus formation and stability. We propose that acquisition of the BRAF^{V600E} mutation does not necessitate growth arrest, but instead permits melanocytes to toggle between hyperproliferation and mitotic arrest. Our transcriptomic analyses demonstrate that external stimuli can modulate the differentiation state of BRAF^{V600E} melanocytes, orchestrate the expression level of MIR211-5p, and inform which phenotype is triggered by the oncogene – before or after the oncogene is introduced.

The senescence model is largely rooted in seminal work demonstrating that sustained ectopic expression of BRAF^{V600E} induces proliferative arrest in primary human melanocytes[9] - an experiment reproduced by several independent labs[24,25,59,60], including our own[23]. In each of these studies, melanocytes were cultured in TPA containing media. Thus, while observations presented here – that BRAF^{V600E} -induced proliferative arrest is reversible and conditional on the presence of TPA – provide new insights that challenge the senescence model, they do not contradict the data presented in these previous reports.

One inherent limitation of using any *in vitro* approach to investigate the mechanisms underlaying clinical phenomena is an inherent incongruity in the magnitude of duration. Melanocytic nevi frequently persist for several decades, whereas *in vitro* experiments are generally conducted on the order of days to weeks. In previous *in vitro* studies, the periods of time melanocytes were monitored subsequent to BRAF^{V600E} introduction ranged from one to three weeks. In studies utilizing an inducible RAF in human fibroblasts, 24 hours of expression was sufficient to drive a durable proliferative arrest, even upon removal of the oncogene[17]. In this study, we induced growth arrest with high levels of BRAF^{V600E} for thirty days and observed the arrest was still reversible. It remains possible that an even longer exposure to BRAF^{V600E} would elicit a permanent proliferative arrest consistent with senescence. It is noteworthy, however, that the identified mechanisms driving proliferative arrest *in vitro* were also supported by analyses of clinical nevi specimens.

While supported by analyses of both primary human melanocytes and clinical specimens, one limitation to this report is the lack of *in vivo* confirmation using animal models. One well-established genetically engineered mouse model of melanoma expresses $BRAF^{V600E}$ from the endogenous locus in tyrosinase expressing cells with spatiotemporal control. The predominant phenotype of $BRAF^{V600E}$ activation in this model is melanocytic hyperplasia, which increases in prominence with $BRAF^{V600E}$ dose[6]. While growth-arrested melanocytic "nevus-like" lesions also form in this model, they are not associated with markers of senescence[8]. More recently, an elegant study utilizing a zebrafish model of melanoma demonstrated that driving $BRAF^{V600E}$ expression from promoters associated with melanocyte progenitors, but not differentiated melanocytes, resulted in melanoma initiation[61]. These observations are all consistent with our data and support the conclusion that $BRAF^{V600E}$-induced proliferation in melanocytes is dependent on differentiation state.

The presented model offers an explanation for several clinical phenomena. First, melanocytic nevi form when $BRAF^{V600E}$ drives hyperproliferation followed by proliferation arrest. Second, nevus eruption involves expansion of previously stable nevi over a short period of time. Third, incomplete excision of melanocytic nevi can result in subsequent regrowth of the benign lesion[18]. Each event requires modulation of the $BRAF^{V600E}$ melanocyte between a proliferative and arrested phase. Our data demonstrate that $BRAF^{V600E}$ melanocytes can indeed oscillate between proliferative and arrested states and are consistent with each of these phenomena. Our interpretation assumes that once acquired, $BRAF^{V600E}$ expression is constant and that the environmental context of the melanocytes is variable, serving as a "gatekeeper" to $BRAF^{V600E}$-induced proliferation. However, if $BRAF^{V600E}$ expression also fluctuates, then an equally plausible interpretation of our data is that $BRAF^{V600E}$ serves as a "gatekeeper" to environmentally induced proliferation. Interestingly, nevus eruption has been observed in metastatic melanoma patients treated with single agent selective BRAF inhibitors[62–66], consistent with our observation that proliferation arrest in melanocytes requires sustained expression of the oncogene. A more thorough understanding of the responsible environmental stimuli in physiologic conditions, discussed in more detail below, would help to clarify which of the mechanisms – variable $BRAF^{V600E}$, variable environment, or both – underlie nevus formation, eruption and recurrence.

It is important to note that while our data support a model of reversible proliferation arrest in nevi, we do not suggest this reversal is commonplace. Unquestionably, the vast majority of melanocytic nevi present with sustained arrest. However, we do propose that the duration of arrest is dynamic and modulated by exposure to external signals. Since our data suggest that loss of MIR211-5p and MIR328-3p expression and restoration of AURKB expression is concurrent with progression to melanoma, identification of the source of cell-extrinsic signals might suggest new strategies for chemoprevention or therapy. We have identified TPA, a known activator of PKC signaling, as one extrinsic factor that induces expression of

560 MIR211-5p and a more dedifferentiated state. Previous studies have identified TPA as either a mitogen,
561 inhibitor of the G1/S transition, or inhibitor of the G2/M transition, dependent on the context[39,40,67–69]. We
562 demonstrate that *in vitro*, TPA activation of MIR211-5p is required for $BRAF^{V600E}$-induced mitotic failure.
563 Yet, the inclusion of TPA in primary melanocyte culture is artificial and the environmental stimulus that
564 regulates MIR211-5p expression in skin remains unknown. One hypothesis is that PKC activation from
565 keratinocyte interactions serves as the extrinsic stimulus. MIR211-5p is reported to be transcriptionally
566 regulated by both MITF[70] and UV exposure[71]. However, TPA-free media containing an endothelin
567 receptor type B ligand, endothelin-1, did not elicit MIR211-5p expression or $BRAF^{V600E}$ arrest, suggestive
568 that the downstream signaling pathways regulated by the two molecules are not identical. PKC activation
569 can also result in increased MAPK signaling[72,73] raising the possibility that internal MAPK fluctuations may
570 play a role in toggling between $BRAF^{V600E}$-induced proliferation versus arrest. The term "mitogenic
571 window" describes the specific range of oncogene doses that elicit a hyperproliferative phenotype. The
572 mitogenic window for MAPK signaling activation can be remarkably fine. Here, we conducted a two-fold
573 dilution series of doxycycline but observed no evidence of a mitogenic window. However, it remains
574 possible that we simply missed the "sweet spot" in TPA conditions, and that a finer dilution series would
575 reveal a mitogenic window even in the presence of TPA. Regardless, our data demonstrate that in TPA
576 conditions the mitogenic window for $BRAF^{V600E}$ expression is, at least, exceedingly narrow, whereas in
577 non-TPA conditions the window is wide open. An important future direction will be to identify the nature
578 and physiological source of this signal for melanocytic nevi in human skin.
579
580 Diminished MIR211-5p/MIR328-3p expression concurrent with increased AURKB expression occurs in a
581 substantial portion of melanomas. AURKB expression was previously reported as significantly elevated in
582 melanoma metastases[45] and here we report increased expression in primary melanomas. Similarly,
583 MIR211-5p expression is consistently observed as lost in melanoma as compared to melanocytic nevi
584 across independent studies[27–29]. Indeed, MIR211-5p expression levels classify nevi from melanomas with
585 a high degree of accuracy[27,28]. We have reported on the diagnostic potential of MIR328-3p expression as
586 well, although multi-study validation was impeded by the absence of hybridization probes in earlier
587 microarray-based profiling datasets[28]. *In vitro*, we have now demonstrated that inhibition of either miRNA
588 is sufficient to block $BRAF^{V600E}$-induced arrest in melanocytes. These data suggest that mitotic failure
589 serves as a barrier to melanoma progression and is consistent with the genome duplication and copy
590 number alterations associated with invasive melanoma[4,74]. In melanoma, the specific cause of this
591 genomic instability is unknown, but reentry of cells into cell cycle after mitotic failure has been shown to
592 cause genome duplication and accumulation of copy number alterations in other cancers[75]. Further
593 experiments will be necessary to determine whether dysregulation of the spindle checkpoint in nevi
594 contributes directly to the copy number variations present in melanomas.
595

596 In summary, we have identified that BRAF^{V600E} induces a reversible arrest in human melanocytes
597 orchestrated by MIR211-5p/MIR328-3p regulation of AURKB and conditional on the melanocyte
598 differentiation state. We present a mechanistic model that allows for melanocytic nevus formation,
599 eruption and recurrence. Moreover, our observations provide an explanation for the genetic duplication
600 and instability inherent to invasive melanomas and open new directions for novel chemopreventative and
601 therapeutic strategies.
602
603 **Competing Interests**
604 R.L.J and M.L.W are inventors on international patent application no. PCT/US2019/023834 concerning
605 the use of microRNAs investigated in this article as molecular diagnostics for melanoma.
606
607 **Acknowledgments**
608 This work was supported by the National Institutes of Health (DP5OD019787 and R01CA229896 to
609 R.L.J., 5F31CA236377 to A.S.M., P30CA042014 to University of Utah), the University of California, San
610 Francisco Program for Breakthrough Biomedical Research (PBBR) Sandler Fellowship to R.L.J. and the 5
611 for the Fight fellowship to R.L.J. We acknowledge the use of the HCI Shared Resources for Research
612 Informatics (RI), Cancer Biostatistics (CB), High-Throughput Genomics and Bioinformatics Analysis
613 (GBA), and the Biorepository and Molecular Pathology (BMP) Research Histology Section supported by
614 P30CA042014 awarded to HCI from the National Cancer Institute.
615
616 **Author Contributions**
617 A.S.M: Investigation, Formal analysis, Writing – original draft, Visualization, Funding acquisition; R.L.B.:
618 Methodology, Investigation, Resources, Writing – review & editing; H.Z.: Methodology, Investigation,
619 Validation, Writing – review & editing; M.U.: Investigation; K.B.: Investigation; R.T.: Formal analysis; M.C.
620 – Formal analysis; A.H.S.: Data curation, Writing – review & editing; R.A., Writing – review & editing:
621 Resources; S.H.: Conceptualization; D.H.L.: Conceptualization, Writing – review & editing; T.H.M.:
622 Resources; M.W.V.: Conceptualization; D.G.: Resources, Writing – review & editing; M.W.: Resources,
623 Writing – review & editing; U.E.L.: Investigation, Formal Analysis, Resources, Writing – review & editing;
624 R.L.J.: Conceptualization, Formal analysis, Investigation, Writing – original draft; Visualization,
625 Supervision, Funding acquisition.
626
627 **Materials and Methods**
628
629 *Transcriptomic profiling*
630 For FFPE samples, histopathologic review, microdissection, targeted exon sequencing, phylogenetic
631 analysis, and RNA and small RNA sequencing of each tumor area were previously described
632 (phs001550.v2.p1)[23,26,28]. For this study, small RNA reads were aligned to human reference (hg37) with

633 Bowtie[76] and small RNA reference groups (miRBase21) were counted. For mRNA sequencing, reads
634 were aligned to human reference (hg37) with Bowtie2 and counted with HTSeq. Differential expression
635 analysis was performed using DESeq2[77] with p-values adjusted by Benjamini-Hochberg method (p-adj).
636 Previously published RNA sequencing datasets from *Shain et al. 2018* and *Torres, et al.* 2020 were re-
637 analyzed here with DESeq2 the combined for visualization. For RNA profiling from primary melanocytes,
638 total RNA was extracted using TRIzol Reagent (Thermo Fisher, 15596-026) and further purified with the
639 RNeasy Power Clean Pro Cleanup Kit (Qiagen, 13997-50) to remove melanin. For small RNAseq of
640 nevus melanocytes sequencing libraries were constructed with the TailorMix Small RNA Library
641 Preparation Kit (SeqMatic, CA) and sequencing was performed on the Illumina HiSeq2500 platform at
642 single-end 50bp. For small RNAseq of cultured $BRAF^{V600E}$ transduced melanocytes, sequencing libraries
643 were constructed with the Qiagen QIAseq miRNA Library Prep kit and sequencing was performed on the
644 NovaSeq SP platform at paired-end 50bp. For mRNAseq of microRNA mimic nucleofected melanocytes,
645 150bp paired end sequencing was conducted by GeneWiz. For mRNAseq of cultured $BRAF^{V600E}$
646 transduced melanocytes, sequencing libraries were constructed with the Illumina TruSeq Stranded mRNA
647 Library Prep kit and sequencing was performed on the NovaSeq S4 platform at paired-end 150bp.
648
649 *Cell derivation and culture*
650 Benign human melanocytic nevi were excised with informed consent from patient donors at the UCSF
651 Dermatology clinic (San Francisco, CA) or HCI Dermatology clinic according to Institutional Review
652 Board- approved protocols. Nevus tissue was minced and enzymatically dissociated in 1mg/mL
653 collagenase (Sigma 11213857001) and 3.3mg/mL dispase (Sigma, 4942078001) in DMEM (Thermo
654 Fisher, 10569044) for 1 hour at 37ºC. Melanocytes were further isolated by 5- day exposure to 10µg/mL
655 G418 (InvivoGen, ant-gn-1). BRAF status was confirmed via sanger sequencing (Quintarabio) using the
656 primer set: BRAF forward: 5'- GCA CGA CAG ACT GCA CAG GG -3'; BRAF reverse: 5'- AGC GGG CCA
657 GCA GCT CAA TAG -3'. BRAF wildtype (normal) human melanocytes were isolated from de-identified
658 and IRB consented neonatal foreskins or adult skin. Foreskin tissue was incubated overnight at 4ºC in
659 dispase and epithelia were mechanically separated from the dermis the following morning. Epithelial
660 tissue was minced and incubated in 0.25% trypsin (Gibco 25200056) for 4min at 37ºC. Trypsin was
661 quenched and tissue centrifuged at 500xg for 5min at room temperature. The cell/tissue pellet was
662 resuspended in Melanocyte medium (ThermoFisher, M254500) with HMGS (ThermoFisher, S0025) and
663 plated in low volume.
664
665 The 501Mel human melanoma line (Gift from Dr. Boris Bastian, CVCL_4633) were cultured in RPMI with
666 10% Fetal Bovine Serum (FBS, VWR, S107G), 1% Penicillin-Streptomycin (Gibco, 15140122), 1% L-
667 Glutamine (Gibco, 25030149), and 1% Non-Essential Amino Acids (Gibco, 11140050). HCIMel019 was
668 derived from patient-derived xenograft (PDX) tumors propagated in mice. An HCIMel019 (P2)
669 subcutaneous tumor was resected from mouse, minced in digestion buffer (100µM HEPES (Gibco,

670 15630-080), 5% FBS (DENVILLE, FB5001-H), 20µg/ml gentamicin (Gibco, 15710-064), 1x insulin (Gibco,
671 51500-056), and 1mg/ml collagenase IV (Gibco, 17104-019) in DMEM (Gibco, 11965-092)), and digested
672 overnight at 37˚C. Cells were filtered through a 100µm filter (Falcon, 352360) and red blood cells
673 removed with RBC lysis buffer (0.5M EDTA, 0.5M KHCO3 (Sigma, 237205), and 5M NH4CL (Sigma,
674 A9434)). Remaining cells were washed with PBS (Gibco, 10010023), and cultured at 37ºC and 5% CO2
675 in Mel2 media consisting of 80%MCDB153 (Sigma, M7403), 20% L15 (Gibco, 11415-064), 2% FBS
676 (DENVILLE, FB5001-H), 1.68mM CaCL (Sigma, C4901), 1x insulin (Gibco, 51500-056) 5ng/ml EGF
677 (Sigma Aldrich, E9644), 15µg/ml Bovine Pituitary Extract (Gibco 13028-014), and 1x Pen/strep (Gibco,
678 15070-063).
679
680 *Small RNA Nucleofection*
681 Human melanocytes were trypsinized (Gibco, 25300062), quenched, and centrifuged at 300xg. Cells
682 were resuspended in R Buffer (ThermoFisher, MPK1025) at 10,000 cells/µL. 10µL of cell slurry was
683 mixed with miRIDIAN microRNA mimics (Dharmacon: hsa-MIR211-5p C-300566-03-0005, hsa-MIR328-
684 3p C-300695-03-0005, MIRControl 1 CN-001000-01-05 or MIRControl 2 CN-002000-01-05); or On-
685 TargetPlus siRNA (Dharmacon, custom library); at 4µM final concentration and nucleofected using the
686 NEON Transfection System and protocol (Thermo Fisher, MPK5000).
687
688 *Generation of Lentiviral vectors*
689 pTRIPZ-diBRAFV600E was a gift from Todd Ridky[25]. pLVX-AURKB (Addgene #153316) and pLVX-
690 GPR3 (Addgene #153317) were generated by subcloning the respective human cDNA (from Addgene
691 #100142 and #66350) into the MluI and BamHI sites] of the pLVX-Che-hi3 vector (a gift of Sanford
692 Simon)[78]. pLVX-anti-MIR211-5p (Addgene #153318), pLVX-anti-MIR328-3p (Addgene #153319), and
693 pLVX-Che-zsGreen (Addgene #153320) were generated by inserting zsGreen with or without a 3'UTR
694 into the MluI and XbaI sites of the pLVX-Che-hi3 vector. The 3'UTRs contained 7 tandem microRNA
695 binding sites to report and inhibit microRNA function, as previously described[34]. ZsGreen was subcloned
696 from pHIV-zsGreen (gift from Bryan Welm & Zena Werb (Addgene #18121))[79].
697
698 *Lentiviral transduction*
699 $2.75x10^6$ HEK293T cells were plated on 10cm tissue culture dishes and grown for ~24 hours in DMEM
700 with 10% FBS. For each 10cm plate, 5µg lentiviral vector, 3.3µg of pMLV-GagPol and 1.7µg of pVSV-G
701 packaging plasmids were added to 500µL of jetPRIME buffer and 20µL of jetPRIME transfection reagent
702 (Polyplus, 712-60), and transfected according to manufacturer's instructions. 48 hours post-transfection,
703 viral supernatant was collected and filtered using 0.45µm syringe filters (Argos 4395-91). Human
704 melanocytes seeded at $1.0x10^5$ – $2.0x10^5$ cells/well density in 6-well plates were incubated in viral
705 supernatant with 10µg/mL polybrene (Sigma, TR-1003) and centrifuged at 300xg for 60 min at room
706 temperature. The viral supernatant was removed and replaced with growth media. Transduced cells were

707 either selected with puromycin (1μg/mL for 5 days, Sigma P8833) or sorted for mCherry expression using
708 a BD FACSAria II. Cells expressing pTRIPZ-diBRAFV600E were treated with doxycycline (Sigma, D9891)
709 at indicated concentrations.
710
711 *Live Quantitative Phase Imaging*
712 Live quantitative imaging was performed using either the HoloMonitor M4 imaging cytometers (Phase
713 Holographic Imaging, Lund, Sweden) or the Livecyte platform (Phasefocus, Sheffield, UK). Analyses of
714 cell proliferation, dry cell mass, and death were acquired with the M4 platform and analyzed using
715 HStudio (v2.6.3) as previously described[31]. For each experiment, human melanocytes were seeded into
716 6-well plates (Sarstedt, 83.3920) at 100,000 cells/well and either live-imaged or serially imaged as
717 indicated. Analysis of growth rate were acquired with the M4 platform and analyzed using App Suite
718 (v3.2.0.60) as previously described[58]. For each experiment, 100,000 melanocytes, 60,000 501Mel cells or
719 150,000 HCIMel019 cells were plated per well and media containing indicated concentrations of
720 barasertib (AURKB inhibitor; AZD1152-HQPA | AZD2811, Selleckchem, A1147) was added. Cells were
721 imaged for 48-72 hours. Analyses of fluorescent reporters coupled with quantitative phase imaging was
722 conducted using the Livecyte platform and analyzed using Analyze (v3.1) (Phasefocus, Sheffield, UK).
723
724 *EdU assays*
725 Normal human melanocytes were nucleofected with microRNA mimics, LNA microRNA inhibitors, or
726 infected with lentiviral vectors (as above) and seeded in 48-well plates at a density of 50,000 cells/well. 4
727 days post-seeding EdU was added to culture media at a 10μM final concentration. 24 hours after EdU
728 addition, media was removed and cells were stained for EdU incorporation and nuclei using the Click-iT
729 EdU Imaging Kit (Thermo Fisher, C10337) and protocol. Images of EdU and nuclei staining were
730 acquired using the Evos FL microscope and quantified with FIJI.
731
732 *Western Blotting*
733 Protein was collected using RIPA Buffer (Thermo Fisher, 89901) supplemented with HALT Protease
734 Inhibitor (Thermo Fisher, 87786). Immunoblotting was carried out as previously described[23]. Membranes
735 were incubated overnight at 4 °C with primary antibodies at the following dilutions: anti-HSP90 (CST,
736 4874) 1:1000, anti-BRAFV600E (Spring Bioscience Corp, E19292) 1:1000, anti-phosphoERK1/2 (CST,
737 4970) 1:1000, anti-AURKB (Abcam, ab2254) 1:1000. Membranes were washed 4X with TBS and 0.5%
738 Tween20, incubated with HRP-conjugated secondary antibody (1:2000) for 30 minutes at room
739 temperature, and visualized with Lumina Forte Western HRP substrate (Millipore, WBLUF0500).
740
741 *Flow analyses*
742 For assessing DNA content, trypsinized melanocytes (as above) were resuspended in 400 PBS. 1mL -20
743 ºC 200 proof ethanol was added dropwise while gently vortexing to achieve 70% final concentration for

744 fixation and incubated overnight at -30 ºC. Cells were centrifuged at 800xg for 5 min, washed with fresh
745 PBS, and incubated in 500µL FxCycle PI/RNase Staining Solution (Invitrogen, F10797) for 20 min at 37
746 ºC. Data were collected on the Fortessa (BD) at low speed and analyzed with FlowJo v10.7.1. Annexin
747 V/PI staining was performed by trypsinizing melanocytes as above. Cells were washed with PBS and
748 resuspended with Annexin V binding buffer (BioLegend, 422201) at a concentration of 1X10^6 cell/mL.
749 5µL APC Annexin V antibody (BioLegend, 640919) and 10µL PI were added. Cells were gently vortexed
750 and incubated in the dark at room temperature for 15 min. Cells were resuspended in 400µL of Annexin
751 V Binding Buffer. Data were collected on the FACs Verse (BD) and analyzed with FlowJo v10.7.1.
752 Aldehyde dehydrogenase activity was measured first by trypsinizing melanocytes as above and then
753 using the ALDEFLUOR kit (Stemcell Technologies, 01700) as described in the manufacture's protocol.
754
755 *Human nevus and melanoma tissue immunohistochemistry*
756 The archived clinical specimens used in the study were procured with IRB approval from the UCSF
757 Dermatopathology Pathology Service archives. For assessment of AURKB and GPR3 expression, 11
758 melanoma and 11 melanocytic nevi with previous diagnosis were de-identified and re-verified
759 histologically (UEL). For assessment of DNA content, 15 additional melanocytic nevi with previous
760 diagnosis were re-verified histologically (UEL). Tissue was fixed in 10% neutral-buffered formalin,
761 processed, embedded in paraffin, and stained with hematoxylin and eosin. 4µm FFPE sections were
762 stained with AURKB (1:400 dilution, Abcam ab2254) or GPR3 (1:125 dilution, Abnova H00002827-M01)
763 antibodies. UEL reviewed immunohistochemical stains with semiquantitative grading for GPR3 (0=none;
764 1=patchy positive; 2=strong positive) and AURKB (0=none; 1=rare positive; 2=scattered positive; 3=
765 frequent positive; 4=many positive). For in vitro immunofluorescence, cells were fixed and stained as
766 previously described[80] with AXL (1:250 dilution, Cell Signaling #8661) or MLANA (1:100, Abcam ab731).
767
768 *Statistical analyses*
769 For differential gene expression, p values were calculated with the DESeq2 (v1.30.1) default Wald test
770 adjusted by the Benjamini-Hochberg method using a 5% false discovery rate (FDR)[81]. Pathway analyses
771 were analyzed using the fast gene set enrichment package[82] in R with a 10% FDR. Gene set enrichment
772 analyses were conducted using GSEA (v4.0.3, Broad Institute) Preranked tool with 1000 permutations.
773 For *in vitro* experiments, pilot studies were initially conducted in triplicate. The required minimal sample
774 size to assess the difference between independent means with independent standard deviations with an
775 alpha error probability of 0.05 and a power of 0.95 was calculated using G*Power (v. 3.1.9.4). P-values
776 were calculated using either paired or unpaired two-tailed T Tests or Wilcoxon tests via Prism 8
777 (Graphpad) as indicated in figure legends.
778
779 *Experimental set-up*

780 For cohorts of clinical specimens, sample number (n) refers to the number of specimens, each from a
781 different patient. For *in vitro* experiments, n refers to independent experiments conducted on different
782 days. In cases where fresh primary melanocytes were used, the cells in each experiment are derived from
783 an independent donor. In cases where cell lines are used, the cells in each experiment represent a
784 different passage and/or day of that line. For different conditions within experiments, replicate wells were
785 plated and arbitrarily chosen for each condition (e.g. not treated versus treated; different concentrations of
786 a compounds, etc.). All data were included.
787
788 *Ethics statement*
789 The archived clinical specimens used in the study were procured with IRB approval from the UCSF
790 Dermatopathology Pathology Service archives (11-07951). Fresh human tissue samples used in this
791 study were obtained with informed consent and consent to publish from each patient. Samples were first
792 coded before being provided to the researchers. The study protocol conformed to the ethical guidelines of
793 the Declaration of Helsinki (1975). Samples were processed following standard operating procedures
794 approved by IRB at University of California, San Francisco (16-20299) and at the Huntsman Cancer
795 Institute (00124195).
796
797 *Data availability*
798 The data which support these findings are available within the article and its supplementary files, as well
799 as from the corresponding author upon reasonable request. The sequencing data produced in this
800 manuscript is available from GEO under the accession number GSE150849.
801
802 **References**
803
804 1. Garnett MJ, Marais R. Guilty as charged: B-RAF is a human oncogene. Cancer Cell.
805 2004;6(4):313–9.
806 2. Davies H, Bignell GR, Cox C, Stephens P, Edkins S, Clegg S, Teague J, Woffendin H, Garnett
807 MJ, Bottomley W, Davis N, Dicks E, Ewing R, Floyd Y, Gray K, Hall S, Hawes R, Hughes J,
808 Kosmidou V, Menzies A, Mould C, Parker A, Stevens C, Watt S, Hooper S, Jayatilake H,
809 Gusterson BA, Cooper C, Shipley J, Hargrave D, Pritchard-Jones K, Maitland N, Chenevix-Trench
810 G, Riggins GJ, Bigner DD, Palmieri G, Cossu A, Flanagan A, Nicholson A, Ho JWC, Leung SY,
811 Yuen ST, Weber BL, Seigler HF, Darrow TL, Paterson H, Wooster R, Stratton MR, Futreal PA.
812 Mutations of the BRAF gene in human cancer. Nature. Nature; 2002 Jun 27 [cited 2021 Mar
813 1];417(6892):949–954.
814 3. Pollock PM, Harper UL, Hansen KS, Yudt LM, Stark M, Robbins CM, Moses TY, Hostetter G,
815 Wagner U, Kakareka J, Salem G, Pohida T, Heenan P, Duray P, Kallioniemi O, Hayward NK,
816 Trent JM, Meltzer PS. High frequency of BRAF mutations in nevi. Nat Genet. Nat Genet; 2003 Jan

817 1 [cited 2021 Mar 1];33(1):19–20.
818 4. Shain AH, Yeh I, Kovalyshyn I, Sriharan A, Talevich E, Gagnon A, Dummer R, North J, Pincus L,
819 Ruben B, Rickaby W, D'Arrigo C, Robson A, Bastian BC. The Genetic Evolution of Melanoma
820 from Precursor Lesions. N Engl J Med. Massachussetts Medical Society; 2015 Nov 12 [cited 2020
821 Jun 27];373(20):1926–1936.
822 5. Bastian BC. The molecular pathology of melanoma: An integrated taxonomy of melanocytic
823 neoplasia. Annu Rev Pathol Mech Dis. Annual Reviews Inc.; 2014 [cited 2020 Aug 21];9:239–271.
824 6. Dankort D, Curley DP, Cartlidge RA, Nelson B, Karnezis AN, Damsky Jr WE, You MJ, DePinho
825 RA, McMahon M, Bosenberg M. BrafV600E cooperates with Pten loss to induce metastatic
826 melanoma. Nat Genet. 2009 May 12 [cited 2019 Jul 17];41(5):544–552.
827 7. Damsky W, Micevic G, Meeth K, Muthusamy V, Curley DP, Santhanakrishnan M, Erdelyi I, Platt
828 JT, Huang L, Theodosakis N, Raza Zaidi M, Tighe S, Davies MA, Dankort D, McMahon M, Merlino
829 G, Bardeesy N, Bosenberg M. mTORC1 activation blocks brafV600E-induced growth arrest but is
830 insufficient for melanoma formation. Cancer Cell. Cell Press; 2015;27(1):41–56.
831 8. Ruiz-Vega R, Chen CF, Razzak E, Vasudeva P, Krasieva TB, Shiu J, Caldwell MG, Yan H,
832 Lowengrub J, Ganesan AK, Lander AD. Dynamics of nevus development implicate cell
833 cooperation in the growth arrest of transformed melanocytes. Elife. eLife Sciences Publications
834 Ltd; 2020 Oct 1 [cited 2021 Mar 1];9:1–24.
835 9. Michaloglou C, Vredeveld LCW, Soengas MS, Denoyelle C, Kuilman T, van der Horst CMAM,
836 Majoor DM, Shay JW, Mooi WJ, Peeper DS. BRAFE600-associated senescence-like cell cycle
837 arrest of human naevi. Nature. 2005 Aug 4 [cited 2019 Jul 17];436(7051):720–724.
838 10. He S, Sharpless NE. Senescence in Health and Disease [Internet]. Cell. Cell Press; 2017 [cited
839 2021 Mar 2]. p. 1000–1011.
840 11. Roy AL, Sierra F, Howcroft K, Singer DS, Sharpless N, Hodes RJ, Wilder EL, Anderson JM. A
841 Blueprint for Characterizing Senescence. Cell. Cell Press; 2020 Nov 25 [cited 2021 Mar
842 2];183(5):1143–1146.
843 12. Serrano M, Lin AW, McCurrach ME, Beach D, Lowe SW. Oncogenic ras provokes premature cell
844 senescence associated with accumulation of p53 and p16(INK4a). Cell. Cell Press; 1997 Mar 7
845 [cited 2021 Mar 2];88(5):593–602.
846 13. Campisi J, D'Adda Di Fagagna F. Cellular senescence: When bad things happen to good cells
847 [Internet]. Nature Reviews Molecular Cell Biology. Nat Rev Mol Cell Biol; 2007 [cited 2021 Mar 2].
848 p. 729–740.
849 14. Collado M, Serrano M. The power and the promise of oncogene-induced senescence markers
850 [Internet]. Nature Reviews Cancer. Nat Rev Cancer; 2006 [cited 2021 Mar 2]. p. 472–476.
851 15. Afshari CA, Vojta PJ, Annab LA, Futreal PA, Willard TB, Barrett JC. Investigation of the role of
852 G1/S cell cycle mediators in cellular senescence. Exp Cell Res. Exp Cell Res; 1993 [cited 2021
853 Mar 2];209(2):231–237.

854 16. Chatsirisupachai K, Palmer D, Ferreira S, de Magalhães JP. A human tissue-specific
855 transcriptomic analysis reveals a complex relationship between aging, cancer, and cellular
856 senescence. Aging Cell. Blackwell Publishing Ltd; 2019 Dec 1 [cited 2021 Mar 2];18(6).
857 17. Zhu J, Woods D, McMahon M, Bishop JM. Senescence of human fibroblasts induced by
858 oncogenic Raf. Genes Dev. Cold Spring Harbor Laboratory Press; 1998 Oct 1 [cited 2021 Mar
859 1];12(19):2997–3007.
860 18. King R, Hayzen BA, Page RN, Googe PB, Zeagler D, Mihm MC. Recurrent nevus phenomenon: A
861 clinicopathologic study of 357 cases and histologic comparison with melanoma with regression.
862 Mod Pathol. Mod Pathol; 2009 May [cited 2021 Mar 2];22(5):611–617.
863 19. Burian EA, Jemec GBE. Eruptive Melanocytic Nevi: A Review. Am J Clin Dermatol. 2019 May 22
864 [cited 2019 Jun 21];20(5):669–682.
865 20. Cotter MA, Florell SR, Leachman SA, Grossman D. Absence of senescence-associated β-
866 galactosidase activity in human melanocytic nevi in vivo [3] [Internet]. Journal of Investigative
867 Dermatology. J Invest Dermatol; 2007 [cited 2021 Mar 2]. p. 2469–2471.
868 21. Tran SL, Haferkamp S, Scurr LL, Gowrishankar K, Becker TM, Desilva C, Thompson JF, Scolyer
869 RA, Kefford RF, Rizos H. Absence of distinguishing senescence traits in human melanocytic nevi.
870 J Invest Dermatol. Nature Publishing Group; 2012 [cited 2021 Mar 2];132(9):2226–2234.
871 22. Oaxaca G, Billings SD, Ko JS. p16 Range of expression in dermal predominant benign epithelioid
872 and spindled nevi and melanoma. J Cutan Pathol. Blackwell Publishing Ltd; 2020 Sep 6 [cited
873 2021 Mar 2];47(9):815–823.
874 23. Zeng H, Jorapur A, Shain AH, Lang UE, Torres R, Zhang Y, McNeal AS, Botton T, Lin J, Donne
875 M, Bastian IN, Yu R, North JP, Pincus L, Ruben BS, Joseph NM, Yeh I, Bastian BC, Judson RL.
876 Bi-allelic Loss of CDKN2A Initiates Melanoma Invasion via BRN2 Activation. Cancer Cell. Cell
877 Press; 2018 Jul 9 [cited 2021 Mar 2];34(1):56-68.e9.
878 24. Haferkamp S, Scurr LL, Becker TM, Frausto M, Kefford RF, Rizos H. Oncogene-induced
879 senescence does not require the p16 INK4a or p14ARF melanoma tumor suppressors. J Invest
880 Dermatol. J Invest Dermatol; 2009 Aug [cited 2021 Mar 2];129(8):1983–1991.
881 25. McNeal AS, Liu K, Nakhate V, Natale CA, Duperret EK, Capell BC, Dentchev T, Berger SL, Herlyn
882 M, Seykora JT, Ridky TW. CDKN2B loss promotes progression from benign melanocytic nevus to
883 melanoma. Cancer Discov. American Association for Cancer Research Inc.; 2015 Oct 1 [cited
884 2021 Mar 2];5(10):1072–1085.
885 26. Shain AH, Joseph NM, Yu R, Benhamida J, Liu S, Prow T, Ruben B, North J, Pincus L, Yeh I,
886 Judson R, Bastian BC. Genomic and Transcriptomic Analysis Reveals Incremental Disruption of
887 Key Signaling Pathways during Melanoma Evolution. Cancer Cell. 2018 Jul 9 [cited 2019 Jul
888 17];34(1):45-55.e4.
889 27. Babapoor S, Horwich M, Wu R, Levinson S, Gandhi M, Makkar H, Kristjansson A, Chang M,
890 Dadras SS. microRNA in situ hybridization for miR-211 detection as an ancillary test in melanoma

891 diagnosis. Mod Pathol. Nature Publishing Group; 2016 May 1 [cited 2021 Apr 27];29(5):461–475.
892 28. Torres R, Lang UE, Hejna M, Shelton SJ, Joseph NM, Shain AH, Yeh I, Wei ML, Oldham MC,
893 Bastian BC, Judson-Torres RL. MicroRNA Ratios Distinguish Melanomas from Nevi. J Invest
894 Dermatol. Elsevier B.V.; 2020 Jan 1 [cited 2021 Mar 9];140(1):164-173.e7.
895 29. Latchana N, Ganju A, Howard JH, Carson WE. MicroRNA dysregulation in melanoma. Surg
896 Oncol. Elsevier Ltd; 2016 Sep 1 [cited 2021 Mar 9];25(3):184–189.
897 30. Miniotis MF, Mukwaya A, Wingren AG. Digital holographic microscopy for non-invasive monitoring
898 of cell cycle arrest in L929 cells. PLoS One. Public Library of Science; 2014 Sep 1 [cited 2021 Mar
899 9];9(9).
900 31. Hejna M, Jorapur A, Song JS, Judson RL. High accuracy label-free classification of single-cell
901 kinetic states from holographic cytometry of human melanoma cells. Sci Rep. Nature Publishing
902 Group; 2017 Dec 1 [cited 2021 Mar 9];7(1).
903 32. Barker KL, Boucher KM, Judson-Torres RL. Label-Free Classification of Apoptosis, Ferroptosis
904 and Necroptosis Using Digital Holographic Cytometry. Appl Sci. MDPI AG; 2020 Jun 27 [cited
905 2021 Mar 9];10(13):4439.
906 33. Normand G, King RW. Understanding cytokinesis failure. Adv Exp Med Biol. NIH Public Access;
907 2010 [cited 2021 Mar 9];675:27–55.
908 34. Judson RL, Greve TS, Parchem RJ, Blelloch R. MicroRNA-based discovery of barriers to
909 dedifferentiation of fibroblasts to pluripotent stem cells. Nat Struct Mol Biol. Nat Struct Mol Biol;
910 2013 Oct [cited 2020 Aug 30];20(10):1227–1237.
911 35. D'Avino PP, Capalbo L. New auroras on the roles of the chromosomal passenger complex in
912 cytokinesis: Implications for cancer therapies. Front Oncol. Frontiers Media S.A.; 2015 [cited 2021
913 Mar 9];5(OCT).
914 36. Clark AS, Karasic TB, DeMichele A, Vaughn DJ, O'Hara M, Perini R, Zhang P, Lal P, Feldman M,
915 Gallagher M, O'Dwyer PJ. Palbociclib (PD0332991) - A selective and potent cyclin-dependent
916 kinase inhibitor: A review of pharmacodynamics and clinical development [Internet]. JAMA
917 Oncology. American Medical Association; 2016 [cited 2021 Mar 9]. p. 253–260.
918 37. Helfrich BA, Kim J, Gao D, Chan DC, Zhang Z, Tan AC, Bunn PA. Barasertib (AZD1152), a small
919 molecule Aurora B inhibitor, inhibits the growth of SCLC cell lines in vitro and in vivo. Mol Cancer
920 Ther. American Association for Cancer Research Inc.; 2016 Oct 1;15(10):2314–2322.
921 38. Hsu MY, Li L, Herlyn M. Cultivation of normal human epidermal melanocytes in the absence of
922 phorbol esters. Methods Mol Med. Methods Mol Med; 2005 [cited 2021 May 6];107:13–28.
923 39. Coppock DL, Buffolino P, Kopman C, Nathanson L. Inhibition of the melanoma cell cycle and
924 regulation at the G1/S transition by 12-O-tetradecanoylphorbol-13-acetate (TPA) by modulation of
925 CDK2 activity. Exp Cell Res. 1995 Nov [cited 2021 May 6];221(1):92–102.
926 40. Arita Y, Buffolino P, Coppock DL. Regulation of the cell cycle at the G2/M boundary in metastatic
927 melanoma cells by 12-O-tetradecanoyl phorbol-13-acetate (TPA) by blocking p34(cdc2) kinase

928 activity. Exp Cell Res. Academic Press Inc.; 1998 Aug 1 [cited 2021 May 6];242(2):381–390.
929 41. Wellbrock C, Ogilvie L, Hedley D, Karasarides M, Martin J, Niculescu-Duvaz D, Springer CJ,
930 Marais R. V599EB-RAF is an Oncogene in Melanocytes. Cancer Res. Cancer Res; 2004 Apr 1
931 [cited 2021 Mar 9];64(7):2338–2342.
932 42. Mukherji S, Ebert MS, Zheng GXY, Tsang JS, Sharp PA, Van Oudenaarden A. MicroRNAs can
933 generate thresholds in target gene expression. Nat Genet. Nat Genet; 2011 Sep [cited 2021 May
934 6];43(9):854–859.
935 43. Ovando-Vázquez C, Lepe-Soltero D, Abreu-Goodger C. Improving microRNA target prediction
936 with gene expression profiles. BMC Genomics. BioMed Central Ltd.; 2016 May 17 [cited 2021 May
937 6];17(1).
938 44. Ebert MS, Sharp PA. Roles for MicroRNAs in conferring robustness to biological processes
939 [Internet]. Cell. Elsevier B.V.; 2012 [cited 2021 May 6]. p. 515–524.
940 45. Sharma A, Madhunapantula S V., Gowda R, Berg A, Neves RI, Robertson GP. Identification of
941 Aurora Kinase B and Wee1-Like Protein Kinase as Downstream Targets of V600EB-RAF in
942 Melanoma. Am J Pathol. Am J Pathol; 2013 Apr [cited 2021 Apr 27];182(4):1151–1162.
943 46. Liberzon A, Birger C, Thorvaldsdóttir H, Ghandi M, Mesirov JP, Tamayo P. The Molecular
944 Signatures Database Hallmark Gene Set Collection. Cell Syst. Cell Press; 2015 Dec 23 [cited
945 2021 May 6];1(6):417–425.
946 47. Kanehisa M, Sato Y, Kawashima M, Furumichi M, Tanabe M. KEGG as a reference resource for
947 gene and protein annotation. Nucleic Acids Res. Oxford University Press; 2016;44(D1):D457–
948 D462.
949 48. Ryu B, Moriarty WF, Stine MJ, DeLuca A, Kim DS, Meeker AK, Grills LD, Switzer RA, Eller MS,
950 Alani RM. Global Analysis of BRAFV600E Target Genes in Human Melanocytes Identifies Matrix
951 Metalloproteinase-1 as a Critical Mediator of Melanoma Growth. J Invest Dermatol. NIH Public
952 Access; 2011 [cited 2021 Sep 19];131(7):1579.
953 49. Belote RL, Le D, Maynard A, Lang UE, Sinclair A, Lohman BK, Planells-Palop V, Baskin L, Tward
954 AD, Darmanis S, Judson-Torres RL. Human melanocyte development and melanoma
955 dedifferentiation at single-cell resolution. Nat Cell Biol 2021 239. Nature Publishing Group; 2021
956 Sep 2 [cited 2021 Sep 19];23(9):1035–1047.
957 50. Hoek KS, Goding CR. Cancer stem cells versus phenotype-switching in melanoma [Internet].
958 Pigment Cell and Melanoma Research. Pigment Cell Melanoma Res; 2010 [cited 2021 May 6]. p.
959 746–759.
960 51. Tirosh I, Izar B, Prakadan SM, Wadsworth MH, Treacy D, Trombetta JJ, Rotem A, Rodman C,
961 Lian C, Murphy G, Fallahi-Sichani M, Dutton-Regester K, Lin JR, Cohen O, Shah P, Lu D,
962 Genshaft AS, Hughes TK, Ziegler CGK, Kazer SW, Gaillard A, Kolb KE, Villani AC, Johannessen
963 CM, Andreev AY, Van Allen EM, Bertagnolli M, Sorger PK, Sullivan RJ, Flaherty KT, Frederick DT,
964 Jané-Valbuena J, Yoon CH, Rozenblatt-Rosen O, Shalek AK, Regev A, Garraway LA. Dissecting

965 the multicellular ecosystem of metastatic melanoma by single-cell RNA-seq. Science (80-).
966 American Association for the Advancement of Science; 2016 Apr 8 [cited 2021 May
967 6];352(6282):189–196.
968 52. Tsoi J, Robert L, Paraiso K, Galvan C, Sheu KM, Lay J, Wong DJL, Atefi M, Shirazi R, Wang X,
969 Braas D, Grasso CS, Palaskas N, Ribas A, Graeber TG. Multi-stage Differentiation Defines
970 Melanoma Subtypes with Differential Vulnerability to Drug-Induced Iron-Dependent Oxidative
971 Stress. Cancer Cell. Cell Press; 2018 May 14 [cited 2021 May 6];33(5):890-904.e5.
972 53. Haq R, Fisher DE, Widlund HR. Molecular pathways: BRAF induces bioenergetic adaptation by
973 attenuating oxidative phosphorylation. Clin Cancer Res. American Association for Cancer
974 Research Inc.; 2014 May 1 [cited 2021 May 6];20(9):2257–2263.
975 54. S P, T W, PA H, SH K. Stimulation of melanogenesis by tetradecanoylphorbol 13-acetate (TPA) in
976 mouse melanocytes and neural crest cells. Pigment cell Res. Pigment Cell Res; 2003 Feb [cited
977 2021 Sep 19];16(1):26–34.
978 55. Vidács DL, Veréb Z, Bozó R, Flink LB, Polyánka H, Németh IB, Póliska S, Papp BT, Manczinger
979 M, Gáspár R, Mirdamadi S, Kemény L, Bata-Csörgő Z. Phenotypic plasticity of melanocytes
980 derived from human adult skin. Pigment Cell Melanoma Res. John Wiley & Sons, Ltd; 2021 Aug
981 31 [cited 2021 Sep 19];00:1–14.
982 56. Kormos B, Belső N, Bebes A, Szabad G, Bacsa S, Széll M, Kemény L, Bata-Csörgő Z. In Vitro
983 Dedifferentiation of Melanocytes from Adult Epidermis. PLoS One. Public Library of Science; 2011
984 [cited 2021 Sep 19];6(2):17197.
985 57. Rogers T, Marino ML, Raciti P, Jain M, Busam KJ, Marchetti MA, Marghoob AA. Biologically
986 distinct subsets of nevi [Internet]. Giornale Italiano di Dermatologia e Venereologia. Edizioni
987 Minerva Medica; 2016 [cited 2021 Apr 27]. p. 365–384.
988 58. Hafner M, Niepel M, Chung M, Sorger PK. Growth rate inhibition metrics correct for confounders in
989 measuring sensitivity to cancer drugs. Nat Methods. Nature Publishing Group; 2016 Jun 1 [cited
990 2021 Mar 8];13(6):521–527.
991 59. C L, A H, M S, S M. Oncogene activation in melanocytes links reactive oxygen to multinucleated
992 phenotype and senescence. Oncogene. Oncogene; 2008 Nov 27 [cited 2021 Sep
993 19];27(56):7070–7082.
994 60. H L, S L, G Z, LN K, Y Z, JP M, Y H, W Z, J Z, L W, C K, K S, M X, W X, GC K, LM S, J F, PJ Z, M
995 H, X X, W G. Oncogenic BRAF-Mediated Melanoma Cell Invasion. Cell Rep. Cell Rep; 2016 May
996 31 [cited 2021 Sep 19];15(9):2012–2024.
997 61. A B, SJ C, E M, JM W, T T, MM T, SE T, RM W, S S, Y F, NR C, SC P, N S, MV H, T S-V, TH H,
998 Y M, T H, SK T, BS T, E K, RP K, L S, RM W. Developmental chromatin programs determine
999 oncogenic competence in melanoma. Science. Science; 2021 Sep 3 [cited 2021 Sep
1000 19];373(6559).
1001 62. Cohen PR, Bedikian AY, Kim KB. Appearance of New Vemurafenib-associated Melanocytic Nevi

1002 on Normal-appearing Skin: Case Series and a Review of Changing or New Pigmented Lesions in
1003 Patients with Metastatic Malignant Melanoma After Initiating Treatment with Vemurafenib. J Clin
1004 Aesthet Dermatol. Matrix Medical Communications; 2013 May [cited 2021 Apr 27];6(5):27–37.
1005 63. Chen FW, Tseng D, Reddy S, Daud AI, Swetter SM. Involution of eruptive melanocytic nevi on
1006 combination BRAF and MEK inhibitor therapy. JAMA Dermatology. American Medical Association;
1007 2014 Nov 1 [cited 2021 Apr 27];150(11):1209–1212.
1008 64. Chu EY, Wanat KA, Miller CJ, Amaravadi RK, Fecher LA, Brose MS, McGettigan S, Giles LR,
1009 Schuchter LM, Seykora JT, Rosenbach M. Diverse cutaneous side effects associated with BRAF
1010 inhibitor therapy: A clinicopathologic study. J Am Acad Dermatol. J Am Acad Dermatol; 2012 Dec
1011 [cited 2021 Apr 27];67(6):1265–1272.
1012 65. Dalle S, Poulalhon N, Debarbieux S, Zaharia D, Mihm MC, Lacouture ME, Rosen A, Marghoob
1013 AA, Busam KJ, Depaepe L, Bringuier PP, Richez P, Baurain JF, Bressac-de Paillerets B, Balme B,
1014 Thomas L. Tracking of second primary melanomas in vemurafenib-treated patients. JAMA
1015 Dermatology. JAMA Dermatol; 2013 Apr [cited 2021 Apr 27];149(4):488–490.
1016 66. Zimmer L, Hillen U, Livingstone E, Lacouture ME, Busam K, Carvajal RD, Egberts F, Hauschild A,
1017 Kashani-Sabet M, Goldinger SM, Dummer R, Long G V., McArthur G, Scherag A, Sucker A,
1018 Schadendorf D. Atypical melanocytic proliferations and new primary melanomas in patients with
1019 advanced melanoma undergoing selective BRAF Inhibition. J Clin Oncol. J Clin Oncol; 2012 Jul 1
1020 [cited 2021 Apr 27];30(19):2375–2383.
1021 67. Arita Y, O'Driscoll KR, Weinstein IB. Growth of Human Melanocyte Cultures Supported by 12-0-
1022 Tetradecanoylphorbol-13-acetate Is Mediated through Protein Kinase C Activation. Cancer Res.
1023 1992 [cited 2021 May 6];52(16):4514–4521.
1024 68. Stavroulaki M, Kardassis D, Chatzaki E, Sakellaris G, Lindschau C, Haller H, Tosca A, Krasagakis
1025 K. Exposure of normal human melanocytes to a tumor promoting phorbol ester reverses growth
1026 suppression by transforming growth factor beta. J Cell Physiol. J Cell Physiol; 2008 Feb [cited
1027 2021 May 6];214(2):363–370.
1028 69. Chao-Hsing KAO, Hsin-Su YU. A study of the effects of phorbol 12-myristate-13-acetate on cell
1029 differentiation of pure human melanocytes in vitro. Arch Dermatol Res. Springer-Verlag; 1991 Apr
1030 [cited 2021 May 6];283(2):119–124.
1031 70. Mazar J, de Young K, Khaitan D, Meister E, Almodovar A, Goydos J, Ray A, Perera RJ. The
1032 Regulation of miRNA-211 Expression and Its Role in Melanoma Cell Invasiveness. PLoS One.
1033 PLoS One; 2010 [cited 2021 Apr 27];5(11).
1034 71. Su M, Miao F, Jiang S, Shi Y, Luo L, He X, Wan J, Xu S, Lei TC. Role of the
1035 p53-TRPM1/miR-211-MMP9 axis in UVB-induced human melanocyte migration and its potential in
1036 repigmentation. Int J Mol Med. Spandidos Publications; 2020 [cited 2021 Apr 27];45(4):1017–
1037 1026.
1038 72. Herrera R, Hubbell S, Decker S, Petruzzelli L. A role for the MEK/MAPK pathway in PMA-induced

1039 cell cycle arrest: Modulation of megakaryocytic differentiation of K562 cells. Exp Cell Res.
1040 Academic Press Inc.; 1998 Feb 1 [cited 2021 Apr 26];238(2):407–414.
1041 73. Ueda Y, Hirai SI, Osada SI, Suzuki A, Mizuno K, Ohno S. Protein kinase C δ activates the MEK-
1042 ERK pathway in a manner independent of Ras and dependent on Raf. J Biol Chem. J Biol Chem;
1043 1996 [cited 2021 May 6];271(38):23512–23519.
1044 74. Vergara IA, Mintoff CP, Sandhu S, McIntosh L, Young RJ, Wong SQ, Colebatch A, Cameron DL,
1045 Kwon JL, Wolfe R, Peng A, Ellul J, Dou X, Fedele C, Boyle S, Arnau GM, Raleigh J, Hatzimihalis
1046 A, Szeto P, Mooi J, Widmer DS, Cheng PF, Amann V, Dummer R, Hayward N, Wilmott J, Scolyer
1047 RA, Cho RJ, Bowtell D, Thorne H, Alsop K, Cordner S, Woodford N, Leditschke J, O'Brien P,
1048 Dawson SJ, McArthur GA, Mann GJ, Levesque MP, Papenfuss AT, Shackleton M. Evolution of
1049 late-stage metastatic melanoma is dominated by aneuploidy and whole genome doubling. Nat
1050 Commun. Nature Research; 2021 Dec 1 [cited 2021 May 12];12(1).
1051 75. Telentschak S, Soliwoda M, Nohroudi K, Addicks K, Klinz FJ. Cytokinesis failure and successful
1052 multipolar mitoses drive aneuploidy in glioblastoma cells. Oncol Rep. Spandidos Publications;
1053 2015 Apr 1 [cited 2021 Mar 9];33(4):2001–2008.
1054 76. Langmead B, Trapnell C, Pop M, Salzberg SL. Ultrafast and memory-efficient alignment of short
1055 DNA sequences to the human genome. Genome Biol. Genome Biol; 2009 Mar 4 [cited 2021 Apr
1056 27];10(3).
1057 77. Love MI, Huber W, Anders S. Moderated estimation of fold change and dispersion for RNA-seq
1058 data with DESeq2. Genome Biol. BioMed Central Ltd.; 2014 Dec 5 [cited 2021 Apr 27];15(12).
1059 78. Takacs CN, Andreo U, Dao Thi VL, Wu X, Gleason CE, Itano MS, Spitz-Becker GS, Belote RL,
1060 Hedin BR, Scull MA, Rice CM, Simon SM. Differential Regulation of Lipoprotein and Hepatitis C
1061 Virus Secretion by Rab1b. Cell Rep. Elsevier B.V.; 2017 Oct 10 [cited 2021 Apr 27];21(2):431–
1062 441.
1063 79. Welm BE, Dijkgraaf GJP, Bledau AS, Welm AL, Werb Z. Lentiviral Transduction of Mammary
1064 Stem Cells for Analysis of Gene Function during Development and Cancer. Cell Stem Cell. Cell
1065 Stem Cell; 2008 Jan 10 [cited 2021 Apr 27];2(1):90–102.
1066 80. Zeng H, Jorapur A, Shain AH, Lang UE, Torres R, Zhang Y, McNeal AS, Botton T, Lin J, Donne
1067 M, Bastian IN, Yu R, North JP, Pincus L, Ruben BS, Joseph NM, Yeh I, Bastian BC, Judson RL.
1068 Bi-allelic Loss of CDKN2A Initiates Melanoma Invasion via BRN2 Activation. Cancer Cell. 2018 Jul
1069 9 [cited 2019 Jul 17];34(1):56-68.e9.
1070 81. Benjamini Y, Drai D, Elmer G, Kafkafi N, Golani I. Controlling the false discovery rate in behavior
1071 genetics research. Behav Brain Res. Behav Brain Res; 2001 [cited 2021 May 12]. p. 279–284.
1072 82. Korotkevich G, Sukhov V, Budin N, Shpak B, Artyomov M, Sergushichev A. Fast gene set
1073 enrichment analysis. bioRxiv. Cold Spring Harbor Laboratory; 2016 Oct 22 [cited 2021 May
1074 12];060012.
1075

1076
1077 **Supplemental Table Legends**
1078
1079 **Supplemental Table S1 (related to Figure 1b)**
1080 Results of differential expression analyses performed on previously published databases of matched
1081 melanocytic nevi and melanoma-arising-from-nevi.
1082
1083 **Supplemental Table S2 (related to Figure 1c)**
1084 Normalized read counts from small RNA sequencing performed on melanocytes derived from healthy
1085 human skin and melanocytic nevi.
1086
1087 **Supplemental Table S3 (related to Figure 2)**
1088 Results of differential expression analyses performed on primary melanocytes nucleofected with
1089 microRNA or control mimics.
1090
1091 **Supplemental Table S4 (related to Figure 2c)**
1092 Results from siRNA screen for EdU incorporation performed in primary melanocytes. Mean and standard
1093 deviation of triplicate screens shown for each gene. Column D indicates the microRNA predicted to
1094 targeted the gene.
1095
1096 **Table S5 (related to Figure 4)**
1097 Results of differential expression analyses performed on primary melanocytes with or without $BRAF^{V600E}$
1098 in +TPA or TPA-free conditions.
1099
1100 **Table S6 (related to Figure 4)**
1101 Results of GSEA analyses performed on primary melanocytes with or without $BRAF^{V600E}$ in +TPA or TPA-
1102 free conditions.
1103
1104 **Fig_3A_Source and Fig_2J_Source**
1105 Zip files containing raw and annotated images of western blots.
1106
1107

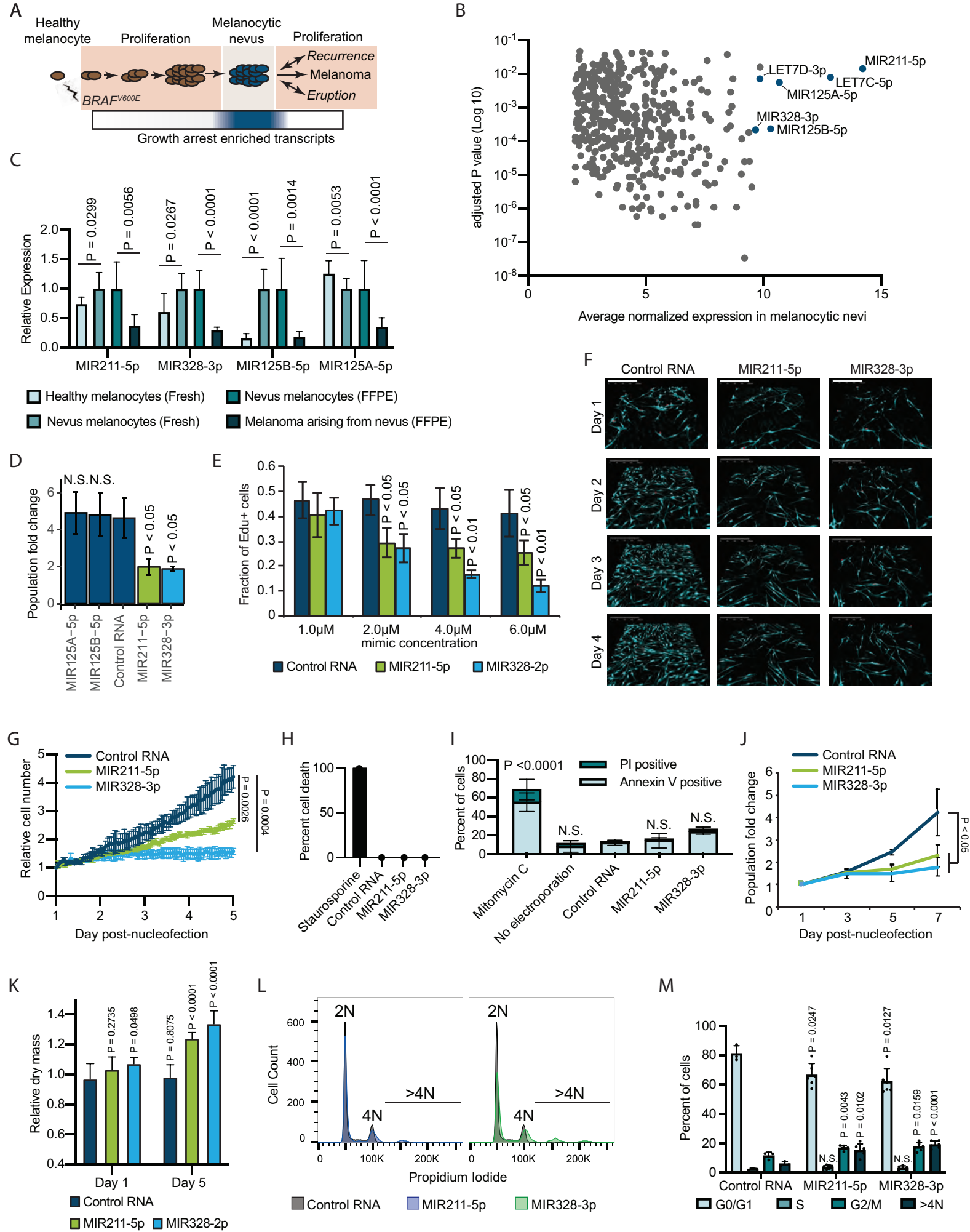
A
Healthy melanocyte
Proliferation
Melanocytic nevus
Proliferation
Recurrence
Melanoma
Eruption
BRAF V600E
Growth arrest enriched transcripts
B
adjusted P value (Log 10)
Average normalized expression in melanocytic nevi
LET7D-3p
MIR211-5p
LET7C-5p
MIR125A-5p
MIR328-3p
MIR125B-5p
C
Relative Expression
P = 0.0299
P = 0.0056
P = 0.0267
P < 0.0001
P < 0.0001
P = 0.0014
P = 0.0053
P < 0.0001
MIR211-5p
MIR328-3p
MIR125B-5p
MIR125A-5p
Healthy melanocytes (Fresh)
Nevus melanocytes (FFPE)
Nevus melanocytes (Fresh)
Melanoma arising from nevus (FFPE)
D
Population fold change
N.S.N.S.
P < 0.05
P < 0.05
MIR125A−5p
MIR125B−5p
Control RNA
MIR211−5p
MIR328−3p
E
Fraction of Edu+ cells
P < 0.05
P < 0.05
P < 0.05
P < 0.01
P < 0.05
P < 0.01
1.0μM
2.0μM
4.0μM
6.0μM
mimic concentration
Control RNA
MIR211-5p
MIR328-2p
F
Control RNA
MIR211-5p
MIR328-3p
Day 1
Day 2
Day 3
Day 4
G
Relative cell number
Control RNA
MIR211-5p
MIR328-3p
P = 0.0026
P = 0.0004
Day post-nucleofection
H
Percent cell death
Staurosporine
Control RNA
MIR211-5p
MIR328-3p
I
Percent of cells
P <0.0001
PI positive
Annexin V positive
N.S.
N.S.
N.S.
Mitomycin C
No electroporation
Control RNA
MIR211-5p
MIR328-3p
J
Population fold change
Control RNA
MIR211-5p
MIR328-3p
P < 0.05
Day post-nucleofection
K
Relative dry mass
P = 0.2735
P = 0.0498
P = 0.8075
P < 0.0001
P < 0.0001
Day 1
Day 5
Control RNA
MIR211-5p
MIR328-2p
L
Cell Count
2N
4N
>4N
Propidium Iodide
Control RNA
MIR211-5p
MIR328-3p
M
Percent of cells
P = 0.0247
P = 0.0043
P = 0.0102
P = 0.0127
P = 0.0159
P < 0.0001
N.S.
N.S.
Control RNA
MIR211-5p
MIR328-3p
G0/G1
S
G2/M
>4N

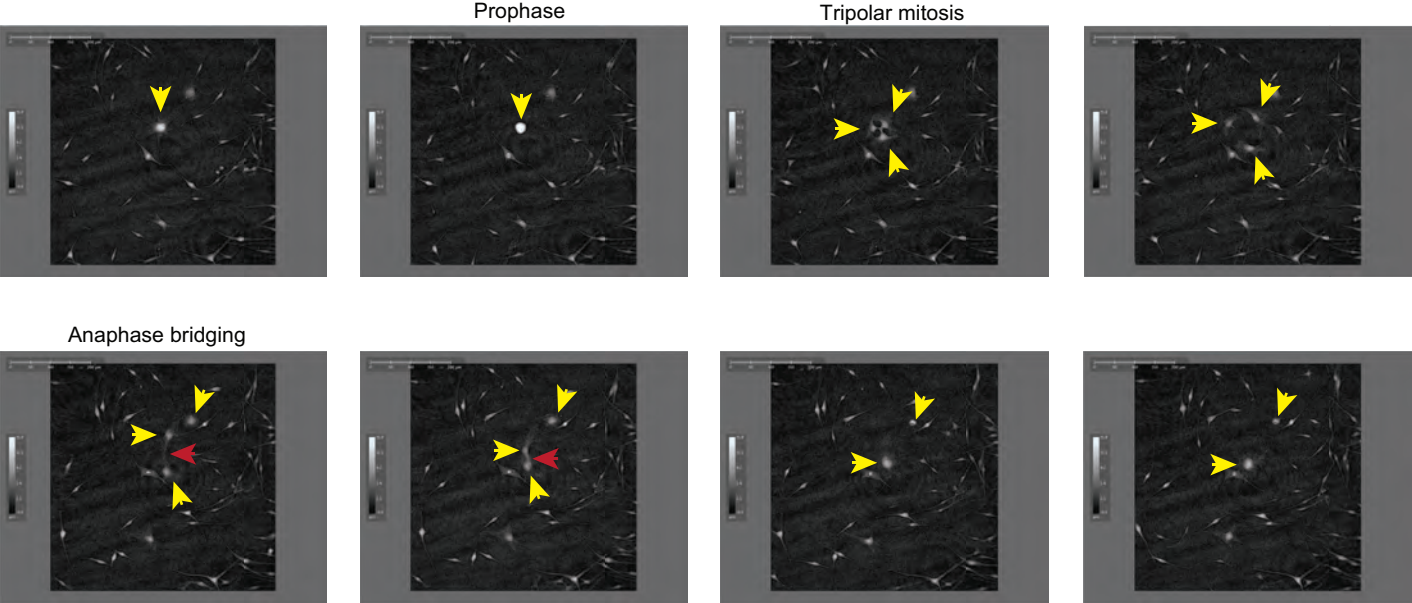
Prophase
Tripolar mitosis
Anaphase bridging

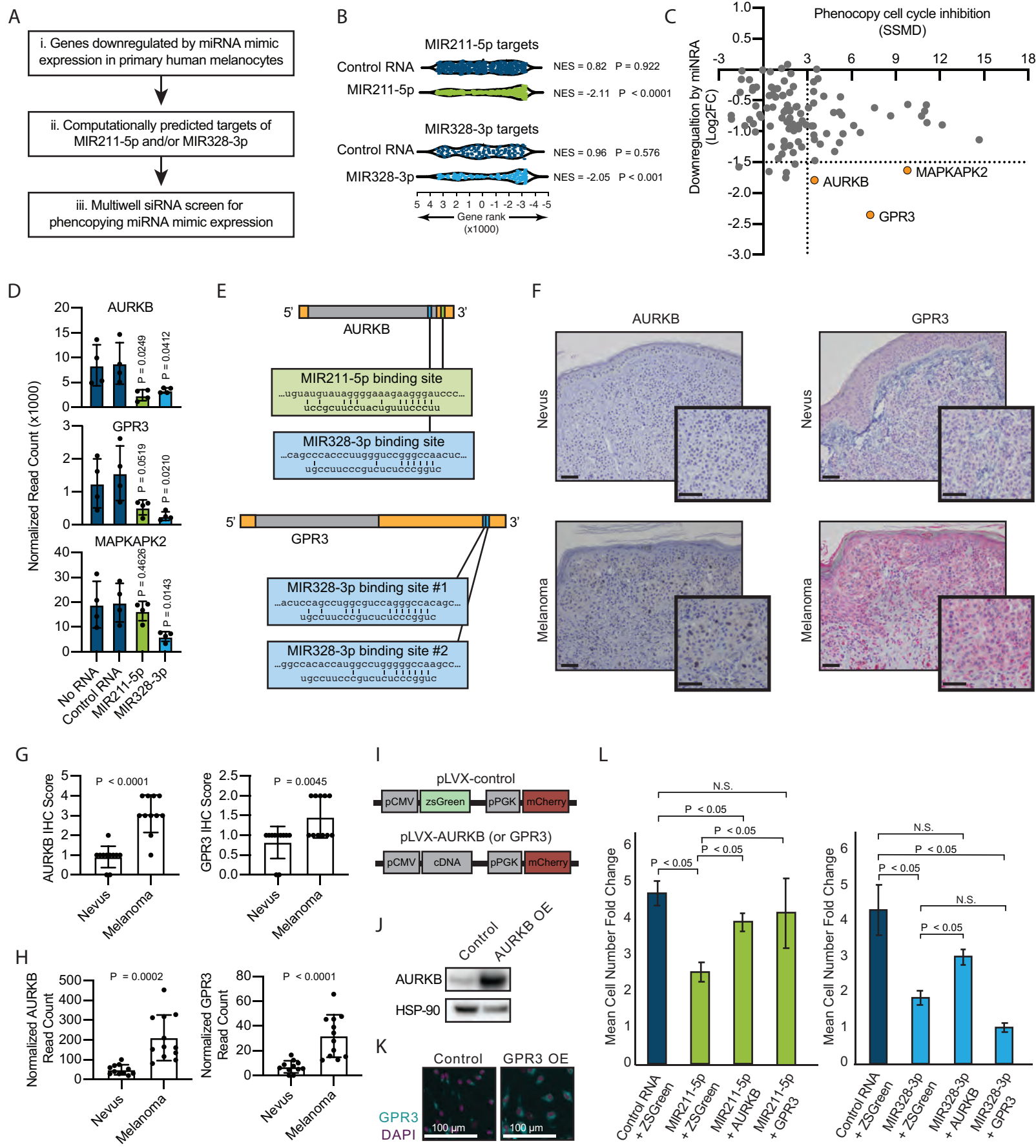
A
i. Genes downregulated by miRNA mimic expression in primary human melanocytes
ii. Computationally predicted targets of MIR211-5p and/or MIR328-3p
iii. Multiwell siRNA screen for phencopying miRNA mimic expression
B
MIR211-5p targets
Control RNA
MIR211-5p
NES = 0.82 P = 0.922
NES = -2.11 P < 0.0001
MIR328-3p targets
Control RNA
MIR328-3p
NES = 0.96 P = 0.576
NES = -2.05 P < 0.001
5 4 3 2 1 0 -1 -2 -3 -4 -5
Gene rank (x1000)
C
Phenocopy cell cycle inhibition (SSMD)
Downregulation by miNRA (Log2FC)
AURKB
MAPKAPK2
GPR3
D
AURKB
GPR3
MAPKAPK2
Normalized Read Count (x1000)
P = 0.0249
P = 0.0412
P = 0.0519
P = 0.0210
P = 0.4626
P = 0.0143
No RNA
Control RNA
MIR211-5p
MIR328-3p
E
5'
3'
AURKB
MIR211-5p binding site
...uguauguauaggggaaagaagggauccc...
uccgcuuccuacuguuucccuu
MIR328-3p binding site
...cagcccacccuuggguccgggccaacuc...
ugccuucccgucucucccgguc
GPR3
MIR328-3p binding site #1
...acuccagccuggcgucccagggccacagc...
ugccuucccgucucucccgguc
MIR328-3p binding site #2
...ggccacaccauggccuggggccaagcc...
ugccuucccgucucucccgguc
F
AURKB
GPR3
Nevus
Melanoma
G
AURKB IHC Score
P < 0.0001
GPR3 IHC Score
P = 0.0045
Nevus
Melanoma
H
Normalized AURKB Read Count
P = 0.0002
Normalized GPR3 Read Count
P < 0.0001
Nevus
Melanoma
I
pLVX-control
pCMV
zsGreen
pPGK
mCherry
pLVX-AURKB (or GPR3)
pCMV
cDNA
pPGK
mCherry
J
Control
AURKB OE
AURKB
HSP-90
K
Control
GPR3 OE
GPR3
DAPI
100 µm
100 µm
L
Mean Cell Number Fold Change
N.S.
P < 0.05
Control RNA + ZSGreen
MIR211-5p + ZSGreen
MIR211-5p + AURKB
MIR211-5p + GPR3
MIR328-3p + ZSGreen
MIR328-3p + AURKB
MIR328-3p + GPR3

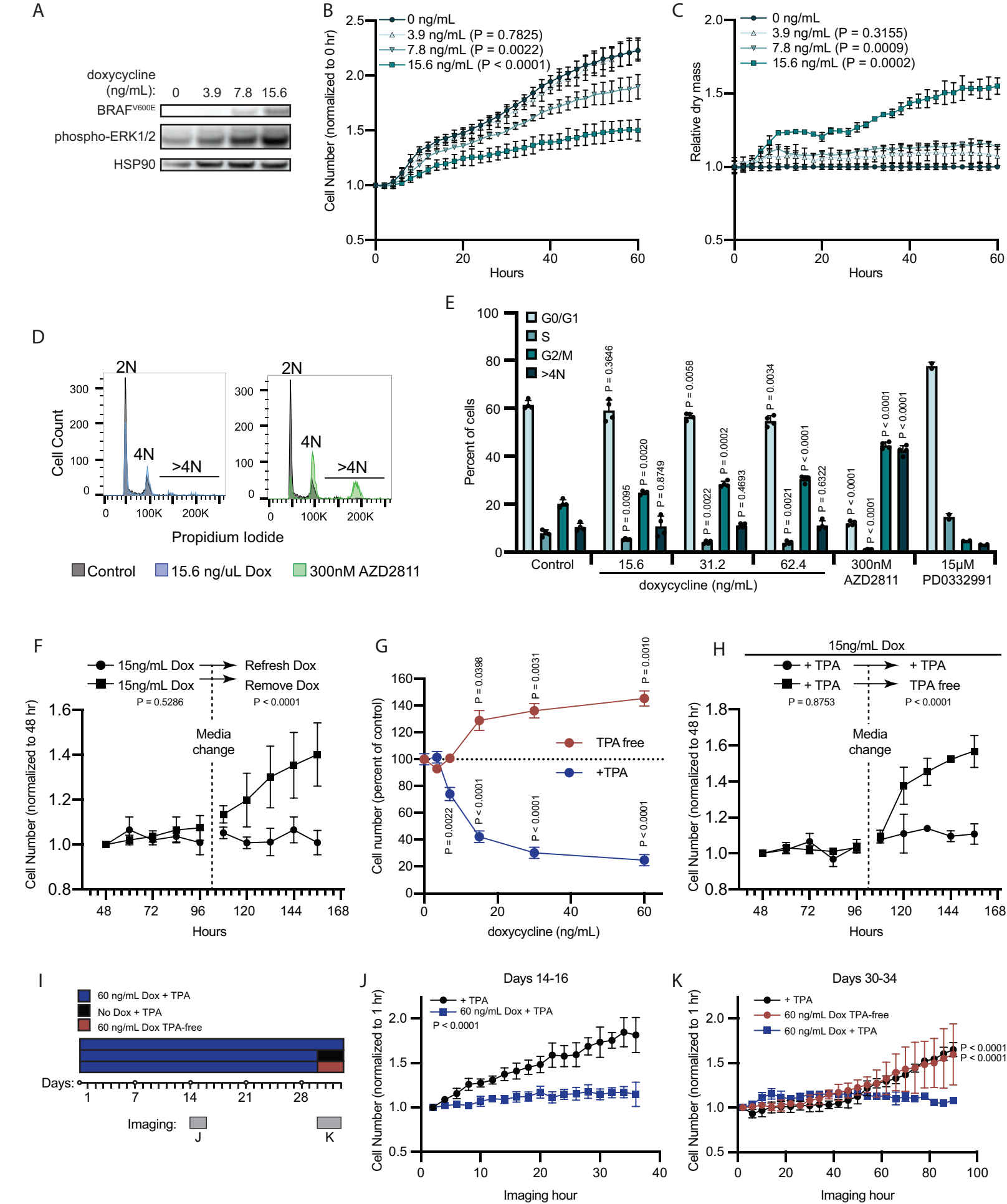
A
doxycycline (ng/mL): 0 3.9 7.8 15.6
BRAF^{V600E}
phospho-ERK1/2
HSP90
B
0 ng/mL
3.9 ng/mL (P = 0.7825)
7.8 ng/mL (P = 0.0022)
15.6 ng/mL (P < 0.0001)
Cell Number (normalized to 0 hr)
Hours
C
0 ng/mL
3.9 ng/mL (P = 0.3155)
7.8 ng/mL (P = 0.0009)
15.6 ng/mL (P = 0.0002)
Relative dry mass
Hours
D
2N
4N
>4N
Cell Count
Propidium Iodide
Control
15.6 ng/uL Dox
300nM AZD2811
E
G0/G1
S
G2/M
>4N
Percent of cells
Control
15.6
31.2
62.4
300nM AZD2811
15μM PD0332991
doxycycline (ng/mL)
F
15ng/mL Dox → Refresh Dox
15ng/mL Dox → Remove Dox
P = 0.5286
P < 0.0001
Media change
Cell Number (normalized to 48 hr)
Hours
G
TPA free
+TPA
Cell number (percent of control)
doxycycline (ng/mL)
H
15ng/mL Dox
+ TPA → + TPA
+ TPA → TPA free
P = 0.8753
P < 0.0001
Media change
Cell Number (normalized to 48 hr)
Hours
I
60 ng/mL Dox + TPA
No Dox + TPA
60 ng/mL Dox TPA-free
Days:
Imaging:
J
K
J
Days 14-16
+ TPA
60 ng/mL Dox + TPA
P < 0.0001
Cell Number (normalized to 1 hr)
Imaging hour
K
Days 30-34
+ TPA
60 ng/mL Dox TPA-free
60 ng/mL Dox + TPA
P < 0.0001
P < 0.0001
Cell Number (normalized to 1 hr)
Imaging hour

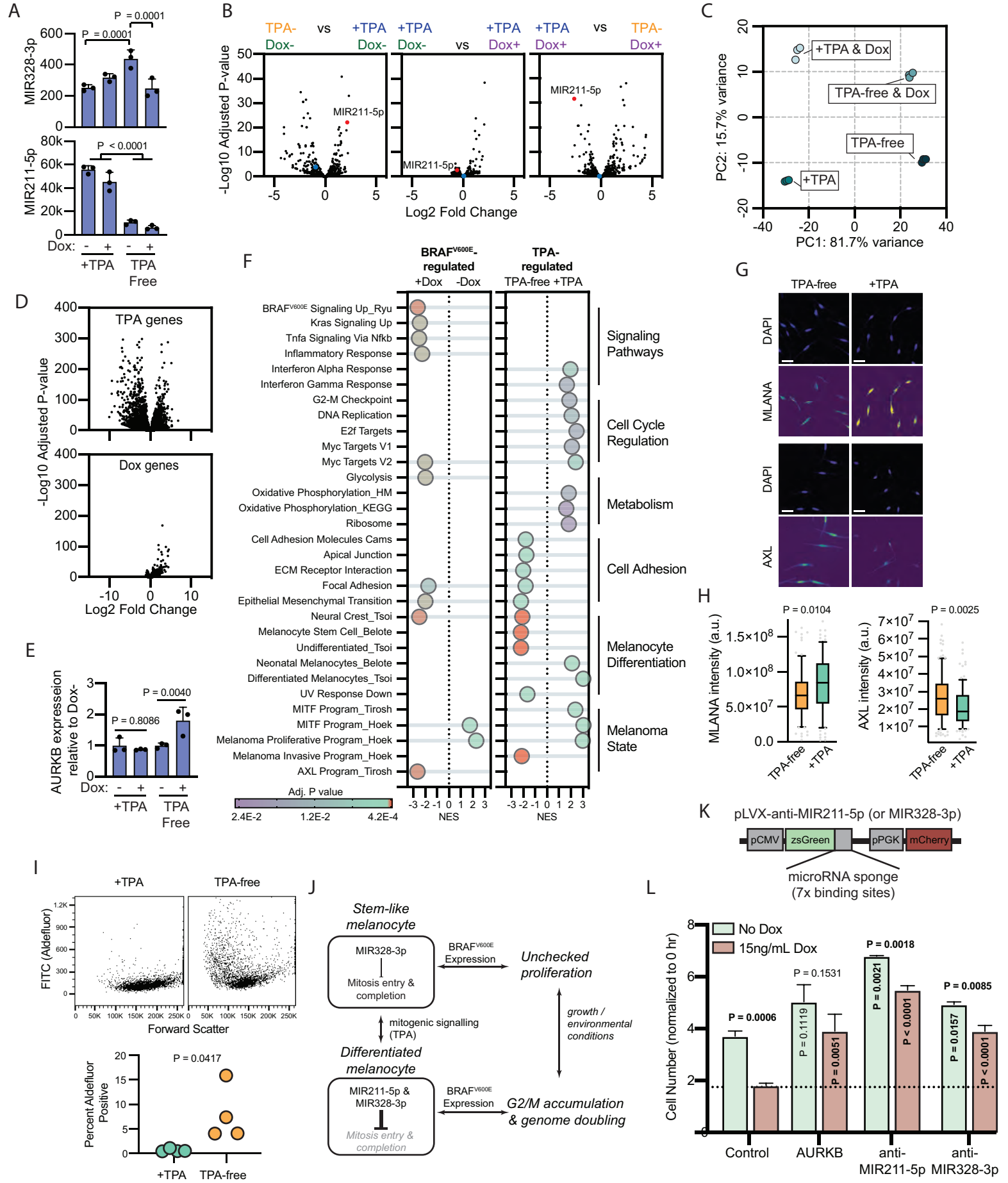
A
P = 0.0001
P = 0.0001
MIR328-3p
MIR211-5p
P < 0.0001
Dox: - + - +
+TPA
TPA Free
B
TPA- Dox- vs +TPA Dox-
+TPA Dox- vs +TPA Dox+
+TPA Dox+ vs TPA- Dox+
-Log10 Adjusted P-value
MIR211-5p
Log2 Fold Change
C
+TPA & Dox
TPA-free & Dox
TPA-free
+TPA
PC2: 15.7% variance
PC1: 81.7% variance
D
TPA genes
Dox genes
-Log10 Adjusted P-value
Log2 Fold Change
E
AURKB expresseion relative to Dox-
P = 0.8086
P = 0.0040
Dox: - + - +
+TPA
TPA Free
F
BRAF V600E-regulated
+Dox -Dox
TPA-regulated
TPA-free +TPA
BRAF V600E Signaling Up_Ryu
Kras Signaling Up
Tnfa Signaling Via Nfkb
Inflammatory Response
Interferon Alpha Response
Interferon Gamma Response
G2-M Checkpoint
DNA Replication
E2f Targets
Myc Targets V1
Myc Targets V2
Glycolysis
Oxidative Phosphorylation_HM
Oxidative Phosphorylation_KEGG
Ribosome
Cell Adhesion Molecules Cams
Apical Junction
ECM Receptor Interaction
Focal Adhesion
Epithelial Mesenchymal Transition
Neural Crest_Tsoi
Melanocyte Stem Cell_Belote
Undifferentiated_Tsoi
Neonatal Melanocytes_Belote
Differentiated Melanocytes_Tsoi
UV Response Down
MITF Program_Tirosh
MITF Program_Hoek
Melanoma Proliferative Program_Hoek
Melanoma Invasive Program_Hoek
AXL Program_Tirosh
Signaling Pathways
Cell Cycle Regulation
Metabolism
Cell Adhesion
Melanocyte Differentiation
Melanoma State
Adj. P value
2.4E-2 1.2E-2 4.2E-4
NES
G
TPA-free +TPA
DAPI
MLANA
AXL
H
P = 0.0104
P = 0.0025
MLANA intensity (a.u.)
AXL intensity (a.u.)
TPA-free
+TPA
I
+TPA
TPA-free
FITC (Aldefluor)
Forward Scatter
P = 0.0417
Percent Aldefluor Positive
J
Stem-like melanocyte
MIR328-3p
Mitosis entry & completion
BRAF V600E Expression
Unchecked proliferation
mitogenic signalling (TPA)
growth / environmental conditions
Differentiated melanocyte
MIR211-5p & MIR328-3p
Mitosis entry & completion
BRAF V600E Expression
G2/M accumulation & genome doubling
K
pLVX-anti-MIR211-5p (or MIR328-3p)
pCMV
zsGreen
pPGK
mCherry
microRNA sponge (7x binding sites)
L
No Dox
15ng/mL Dox
Cell Number (normalized to 0 hr)
P = 0.0006
P = 0.1531
P = 0.1119
P = 0.0051
P = 0.0018
P = 0.0021
P < 0.0001
P = 0.0085
P = 0.0157
P < 0.0001
Control
AURKB
anti-MIR211-5p
anti-MIR328-3p

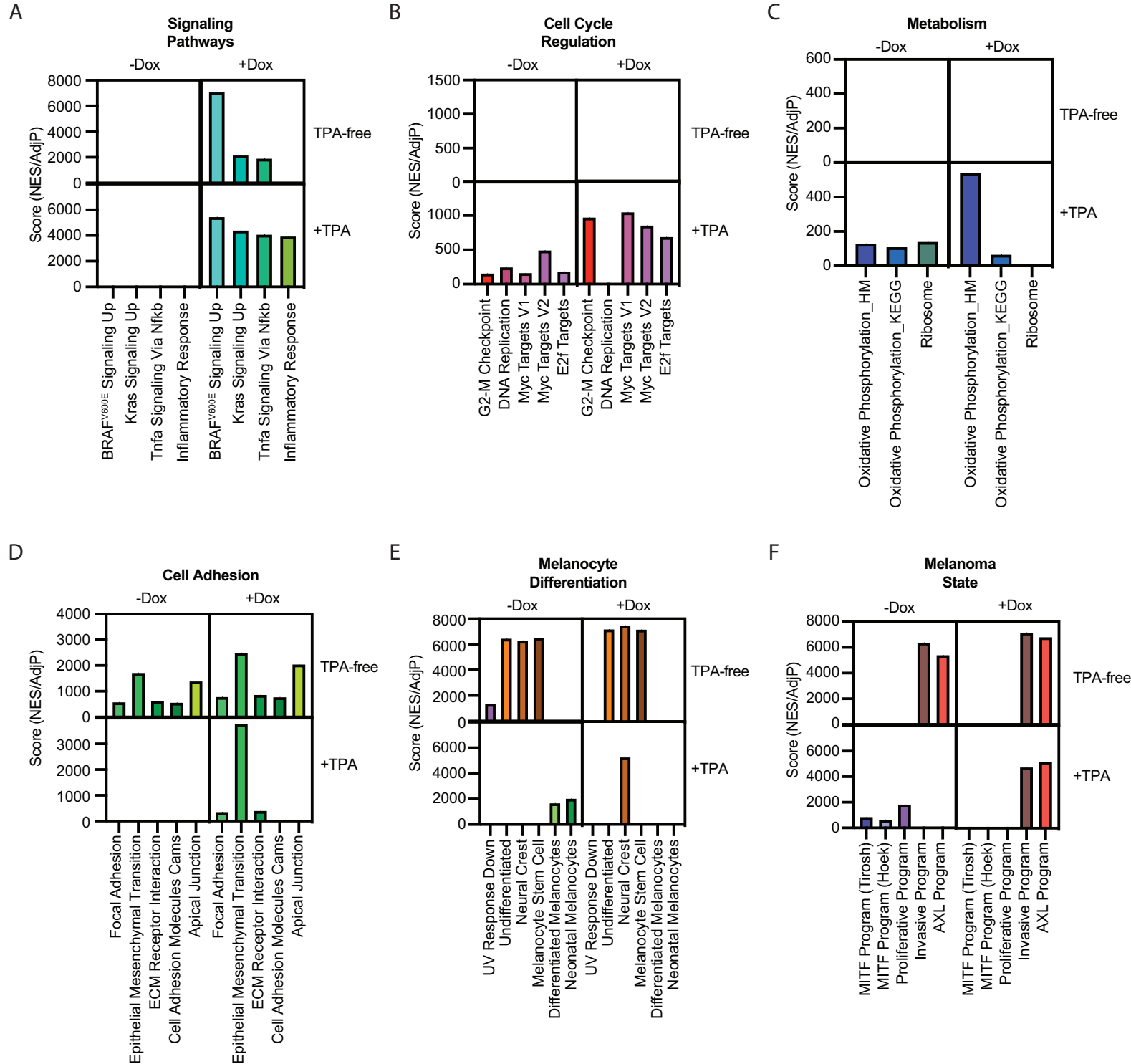
A
Signaling Pathways
-Dox
+Dox
Score (NES/AdjP)
TPA-free
+TPA
BRAF^{V600E} Signaling Up
Kras Signaling Up
Tnfa Signaling Via Nfkb
Inflammatory Response
B
Cell Cycle Regulation
G2-M Checkpoint
DNA Replication
Myc Targets V1
Myc Targets V2
E2f Targets
C
Metabolism
Oxidative Phosphorylation_HM
Oxidative Phosphorylation_KEGG
Ribosome
D
Cell Adhesion
Focal Adhesion
Epithelial Mesenchymal Transition
ECM Receptor Interaction
Cell Adhesion Molecules Cams
Apical Junction
E
Melanocyte Differentiation
UV Response Down
Undifferentiated
Neural Crest
Melanocyte Stem Cell
Differentiated Melanocytes
Neonatal Melanocytes
F
Melanoma State
MITF Program (Tirosh)
MITF Program (Hoek)
Proliferative Program
Invasive Program
AXL Program

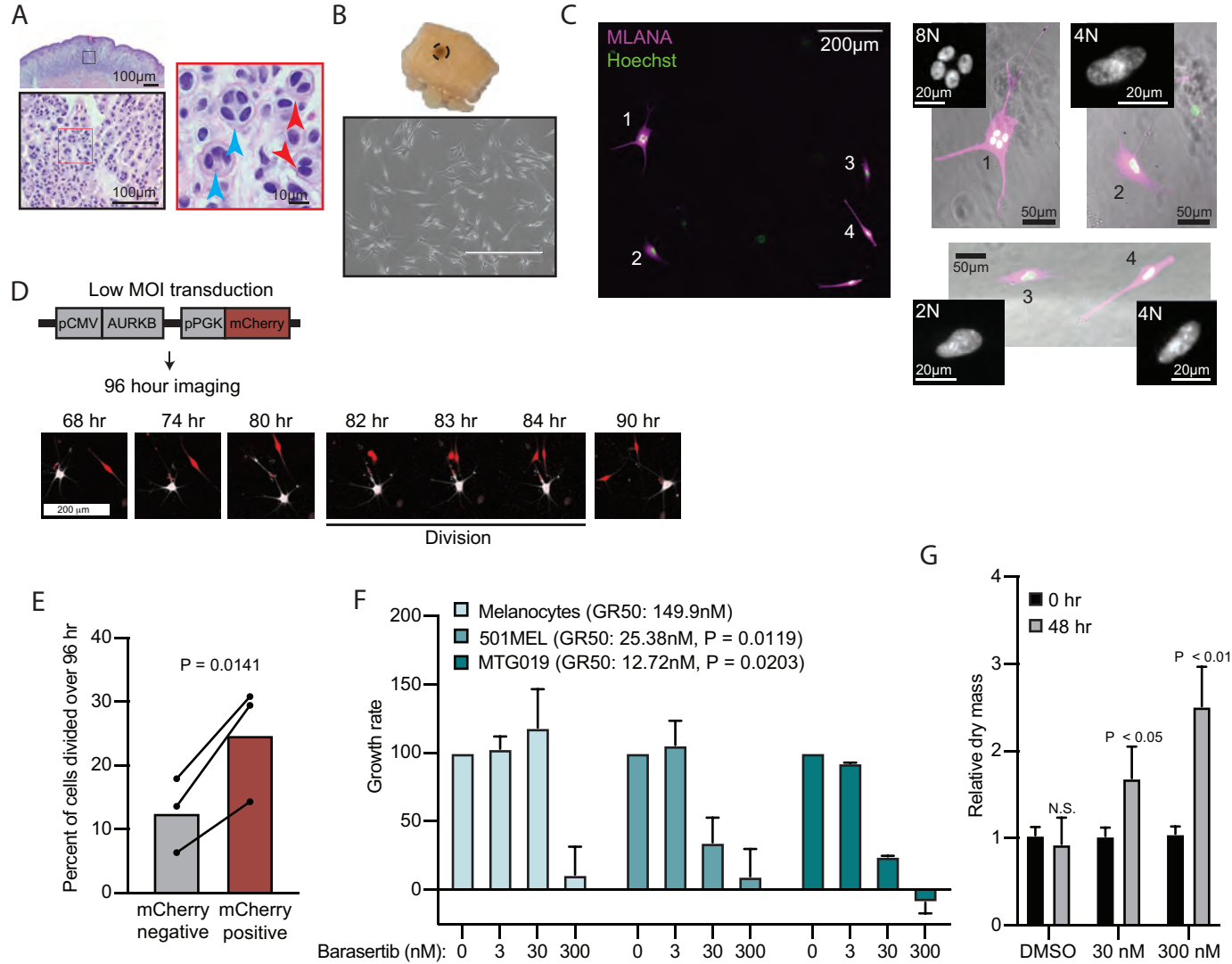
A
100µm
100µm
10µm
B
C
MLANA
Hoechst
200µm
1
2
3
4
8N
4N
2N
20µm
50µm
D
Low MOI transduction
pCMV
AURKB
pPGK
mCherry
96 hour imaging
68 hr
74 hr
80 hr
82 hr
83 hr
84 hr
90 hr
200 µm
Division
E
Percent of cells divided over 96 hr
P = 0.0141
mCherry negative
mCherry positive
F
Melanocytes (GR50: 149.9nM)
501MEL (GR50: 25.38nM, P = 0.0119)
MTG019 (GR50: 12.72nM, P = 0.0203)
Growth rate
Barasertib (nM): 0 3 30 300 0 3 30 300 0 3 30 300
G
0 hr
48 hr
Relative dry mass
N.S.
P < 0.05
P < 0.01
DMSO
30 nM
300 nM